RSC Publishing Organic & Biomolecular Chemistry

Dibenzotetraaza[14]annulene – adenine conjugate recognizes complementary poly dT among ss-DNA / ss-RNA sequences

Journal:	*Organic & Biomolecular Chemistry*
Manuscript ID:	OB-ART-03-2013-040519.R1
Article Type:	Paper
Date Submitted by the Author:	n/a

Complete List of Authors:	Radic Stojkovic, Marijana; Institute Rudjer Boskovic, Division of Organic Chemistry and Biochemistry Skugor, Marko; Institute Rudjer Boskovic, Division of Organic Chemistry and Biochemistry Tomić, Sanja; Institute Rudjer Boskovic, Division of Organic Chemistry and Biochemistry Grabar, Marina; Institute Rudjer Boskovic, Division of Organic Chemistry and Biochemistry Smrecki, Vilko; Rudjer Boskovic Institute, NMR Centre Dudek, Łukasz; Jagiellonian University, Department of Chemistry Grolik, Jarosław; Jagiellonian University, Department of Chemistry Eilmes, Julita; Jagiellonian University, Department of Chemistry Piantanida, Ivo; Rudjer Boskovic Institute, Division of Organic Chemistry and Biochemistry

Dibenzotetraaza[14]annulene – adenine conjugate recognizes complementary poly dT among ss-DNA / ss-RNA sequences.

Marijana Radić Stojković,[a] Marko Škugor,[a] Sanja Tomić,[a] Marina Grabar,[a] Vilko Smrečki,[a] Łukasz Dudek,[b] Jarosław Grolik,[b] Julita Eilmes[b] and Ivo Piantanida[a]*

Received (in XXX, XXX) XthXXXXXXXXX 200X, Accepted Xth XXXXXXXXX 200X
First published on the web Xth XXXXXXXXX 200X
DOI:

Among three novel DBTAA derivatives only DBTAA-propyl-adenine conjugate **1** showed recognition of the consecutive oligo dT sequence by increased affinity and specific induced chirooptical response in comparison to other single stranded RNA and DNA; whereby of particular importance is up until now unique efficient differentiation between dT and rU. At variance, its close analogue DBTAA-hexyl-adenine **2** did not reveal any selectivity among ss-DNA/RNA pointing out to the important role of steric factors (linker length); moreover non-selectivity of the reference compound (**3**, lacking adenine) stressed the importance of adenine interactions in the **1** selectivity.

Introduction

Both, DNA and RNA exhibit a wide range of structural topologies, among which different single stranded (ss–) sequences are quite numerous. While ss–sequences are ubiquitous part of the RNA folding landscape, there are fewer observations of stable ss–DNA cases, such as hairpins[1] or abasic sites,[2] to name some of them. Since ds–DNA is protected from reaction with a number of chemical and biological nucleases,[3] many studies have been aimed at exploiting the vulnerable ss–DNA. A number of small molecules were synthesized that bind specifically at abasic lesions with an idea to inhibit the DNA repair system and in that way pronounce the action of antitumor drugs.[4] Moreover, recently many research groups have explored the potential of the DNA as a template for arraying multichromophoric systems, among which non-covalent ss-DNA-associated dyes attracted considerable attention.[5]

Until now, aryl-nucleobase conjugates efficiently recognized complementary nucleobases by affinity increase,[4] Zn-cyclene derivatives showed highly selective interactions with uracil and thymine caused by specific coordination of Zn with two keto-groups.[6] Very recently, abasic sites and single base bulges in DNA were efficiently recognized by metalloinsertors,[7] or small-ligand-immobilized biosensor was applied for detecting thymine-related single-nucleotide polymorphisms (SNPs).[8] However, longer oligo-dT sequences were not specifically recognised until now, especially in respect to closely related uracil analogues. Within the last decade we showed that small modifications in structure of aryl-nucleobase conjugates can control their selectivity toward various ss- and ds- polynucleotide sequences.[9]

On the other hand, for the dibenzotetraaza[14]annulene (DBTAA) derivatives we recently showed that the interactions of side-chains can finely tune selectivity toward various DNA/RNA and consequently control their biological activity.[10a] Specific properties of the DBTAA moiety, such as larger aromatic surface than the most of until now used aryl-moieties and pronounced out-of-plane flexibility, offered intriguing possibilities in design of novel aryl-nucleobase conjugates. The very last generation of DBTAA derivatives showed high (sub-micromolar) DNA/RNA affinity and selectivity toward dA-dT over dG-dC sequences,[10b] the latter property inspiring us to prepare DBTAA - adenine derivatives (Scheme 1), with the aim of the selective recognition of complementary nucleobases (rU and/or dT) within the DNA/RNA sequences. Previous results showed that structural features of the targeted recognition process sometimes strongly depend on the linker between large aromatic moiety and nucleobase,[9b] therefore we varied the length of the linker between DBTAA and adenine (**1** and **2**), and as the reference compound we prepared the DBTAA lacking nucleobase (**3**).

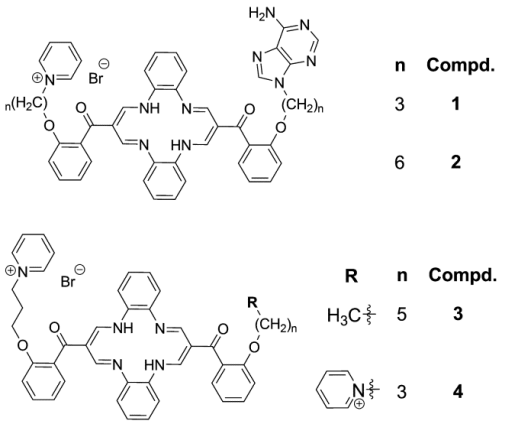

Scheme 1. Novel DBTAA-adenine conjugates **1** and **2** and reference compound **3**, previously studied analogue **4**.[10b,c]

Results and discussion

Synthesis

DBTAA-adenine conjugates **1**, **2** and reference **3** were synthesized via two consecutive monoalkylations by modified

previously described method.[10c] The DBTAA-adenine conjugates **1** and **2** were synthesized in a two-step procedure involving reaction of the bis[2-(3-bromopropoxy)benzoyl]-5,14-dihydrodibenzo[b,i][1,4,8,11]tetraazacyclotetradecine (Scheme 2, a) with adenine in a 1:1 molar ratio, or monoalkylation of bis(2-hydroxybenzoyl)-5,14-dihydrodibenzo[b,i][1,4,8,11]tetraazacyclotetradecine] (Scheme 2, c) using 9-(6-bromohexyl)adenine followed by incorporation of pyridinium - alkoxy moiety according to the method reported earlier.[10c,11] Similar two-step procedure was employed for preparation of unsymmetrically substituted product **3**.

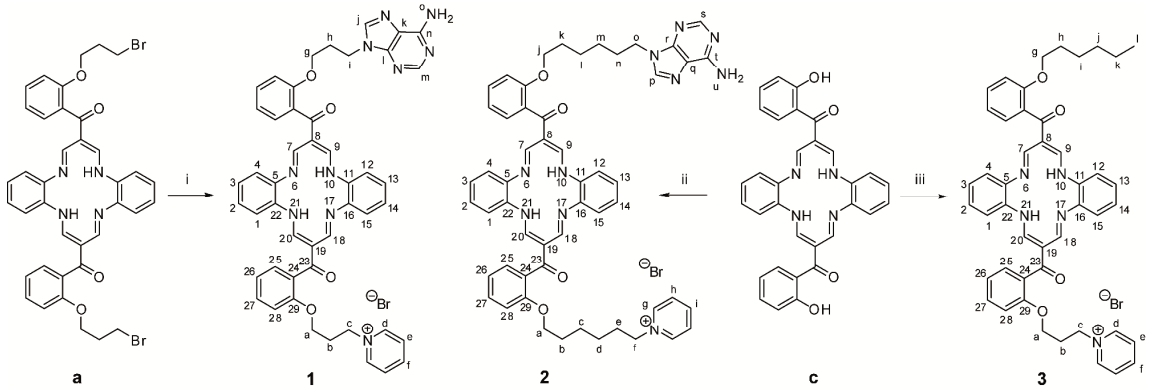

Scheme 2 Starting compounds **a**) and **c**) are prepared as described previously.[10c] Preparation of the products **1**-**3**. i: 1) adenine, NaH, DMF 2) pyridine; ii: 1) 9-(6-bromohexyl)adenine, potassium carbonate, DMF 2) 1,6-dibromohexane, potassium carbonate, DMF 3) pyridine; iii: 1) 1-bromohexane, potassium carbonate, DMF 2) 1,3-dibromopropane, potassium carbonate, DMF 3) pyridine.

Spectroscopic characterisation of buffered solutions of 1-3

Compounds **1-3** were moderately soluble in aqueous solutions (up to c=1 × 10^{-3} mol dm^{-3}). Buffered aqueous solutions of studied compounds were stable for several months. The absorbencies of **1-3** were proportional to their concentrations up to c=1 ×10^{-4} mol dm^{-3}, changes of the UV/vis spectra on the temperature increase up to 95°C were negligible and reproducibility of UV/vis spectra upon cooling back to 25°C was excellent. The UV/vis spectra of **1-3** were similar to previously studied analogue **4**[10c], the differences in molar extinction coefficients† could be attributed to additional adenine chromophore of **1**, **2** and lack of one pyridyl- of **3**.

Study of interactions of 1-3 with ds-DNA in aqueous medium

The experiments with *calf thymus* (ct-)DNA (UV/vis titrations, thermal denaturation, viscometry, gel electrophoresis)† clearly excluded intercalation of DBTAA-adenine conjugates **1-3** into ds-DNA. Only **1** showed induced CD bands at λ > 300 nm upon binding to ct-DNA,† which can be attributed to the well-organized agglomeration within minor groove. At variance to **1-3**, previously studied DBTAA analogue **4**[10b] intercalated into ct-DNA, showing significantly stronger affinity and thermal stabilization effects. Such pronounced difference in the binding mode to ds-DNA could be attributed to distinct structural differences: two positively charged pyridine moieties of **4** are both small enough to allow intercalation of DBTAA into DNA combined with simultaneous electrostatic interactions of two positive charges with negative DNA backbone. At variance to **4**, novel compounds **1, 2** have only one positive charge (thus lowering the attracting forces) and in addition large and neutral adenine of **1**, **2** could by intramolecular stacking on DBTAA compete with intercalation of DBTAA within ds-DNA basepairs. More surprising was non-intercalative binding mode of reference **3**, due to its close similarity to **4**. The differences between **3** and **4** in aqueous solution were significantly lower solubility of former and tendency to form colloidal system upon addition of ct-DNA even at μM concentrations. Particularly latter observation suggested preferred aggregation of **3** along hydrophobic ds-DNA grooves instead of intercalation. However, more detailed studies of **1**-**3** with synthetic ds-DNA/RNA of homogenous basepair composition is necessary prior to any definite conclusion.

Study of interactions of 1-3 with ss-DNA and ss-RNA in aqueous medium

With the idea that DBTAA moiety will easily intercalate within single stranded (ss-) DNA/RNA (much more flexible than ds-DNA), while adenine of **1**, **2** could form H-bonds with complementary nucleobases, we studied interaction of **1-3** with a series of homogeneous RNA and DNA polynucleotides.

Table 1. Binding constants (log*Ks*)[a] calculated from the UV/vis titrations of **1**-**3** with ss- polynucleotides at pH 7.0 (buffer sodium cacodylate, I = 0.05 mol dm^{-3}).

	1		**2**		**3**	
	[c]H / %	log*Ks*	[c]H / %[c]	log*Ks*	[c]H / %	log*Ks*
poly rC	46	6.2 ±0.04	77	5.9±0.03	-[d]	5-6[d]
poly rA	78	5.4 ±0.04	67	5.1±0.02	-[d]	5-6[d]
poly rG	25	6.5 ±0.04	[d]25	5-6[d]	-[d]	5-6[d]
poly rU	59	6.1 ±0.05	[d]62	5-6[d]	-[d]	5-6[d]
poly dT	30	8.7 ±0.04	-[d]	-[d]	-[d]	5-6[d]
polydA	73	5.0 ±0.03	-[d]	-[d]	-[d]	5-6[d]

[a] Processing of titration data by means of Scatchard equation[23] gave values of ratio $n_{[\text{bound } \mathbf{1\text{-}3}]/[\text{polynucleotide}]}$ = 0.2-0.7, for easier comparison all log*Ks* values were re-calculated for fixed n=0.5; [b]Accuracy of n± 10 - 30%, consequently log*Ks* values vary in the same order of magnitude; [c]H_{346nm}=(Abs(**1-3**) - Abs(complex)) / Abs(**1-3**))x 100; [d]Formation of agglomerates close to equimolar concentration of compound and DNA/RNA hampered collection of the sufficient number of data, thus log*Ks* values could be only estimated.

The UV/vis titrations of **1-3** with ss- DNA and ss-RNA revealed pronounced hypochromic effects > 300 nm (Table 1, ESI†), characteristic for aromatic stacking interactions of chromophore (DBTAA) with nucleobases. The affinities of **1-3** toward most of the ss-DNA/RNA were similar, the only exception being intriguing two orders of magnitude higher affinity of **1** toward poly dT (Table 1, Figure 1).

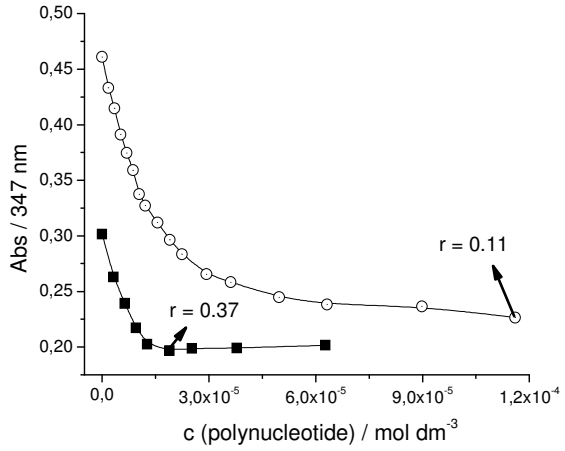

Fig. 1 .Dependence of **1** absorbance at λ_{max}= 347 nm on *c* (■, poly dT) and *c* (○, poly rU), at pH=7, sodium cacodylate buffer, *I* = 0.05 mol dm^{-3}. Ratio r[**1**]/[polynucleotide] at the titration endpoint marked by an arrow.

To get the information about the changes induced by the small molecule on the spectroscopic properties of polynucleotide, the CD spectroscopy was applied as a highly sensitive method to evaluate conformational changes in the secondary structure of polynucleotides.[12] Additionally, the induced (I)CD spectrum which can appear upon binding of achiral small molecules to polynucleotides could give useful information about modes of interaction related to the orientation of a small molecule in respect to the DNA/RNA chiral axis.[12,13] Noteworthy, the **1**-**3** are achiral and therefore do not possess intrinsic CD spectrum. Therefore, we performed CD experiments with **1**-**3**/polynucleotide complexes and indeed, addition of poly dT resulted in the specific induced (I)CD band of **1**, while with other ss-DNA/RNA **1** did not show any ICD band (Figure 2 and ESI†).The plot of ICD band intensity against *c*(poly dT) for **1**/poly dT complex agreed well with UV/vis titration (Fig. 1), supporting high binding constant (Table 1). Such selectivity was not observed for the reference compound **3**, or for the DBTAA-hexyl-adenine **2**, stressing the crucial importance of the adenine as well as the length of a linker connecting it to DBTAA. Apparently, shorter linker of **1** allows much more efficiently intramolecularly-stacked DBTAA-adenine structure, necessary for the fine tuning of the adenine to thymine orientation.

The UV/vis and CD experiments performed with dT decamer revealed also high affinity and the same ICD bands.† However, corresponding experiments of **1**with mononucleotides (AMP, GMP, CMP, UMP, TMP)† yielded at least order of magnitude lower log*Ks* values in comparison to corresponding ss-RNA/DNA (for thymine difference between TMP and poly dT binding constant was 3 orders of magnitude). Moreover, the absence of any ICD band of **1** upon adding aforementioned mononucleotides stressed the essential impact of several consecutive dT in oligonucleotide sequence for achieving the efficient helical organisation and consequent ICD recognition.

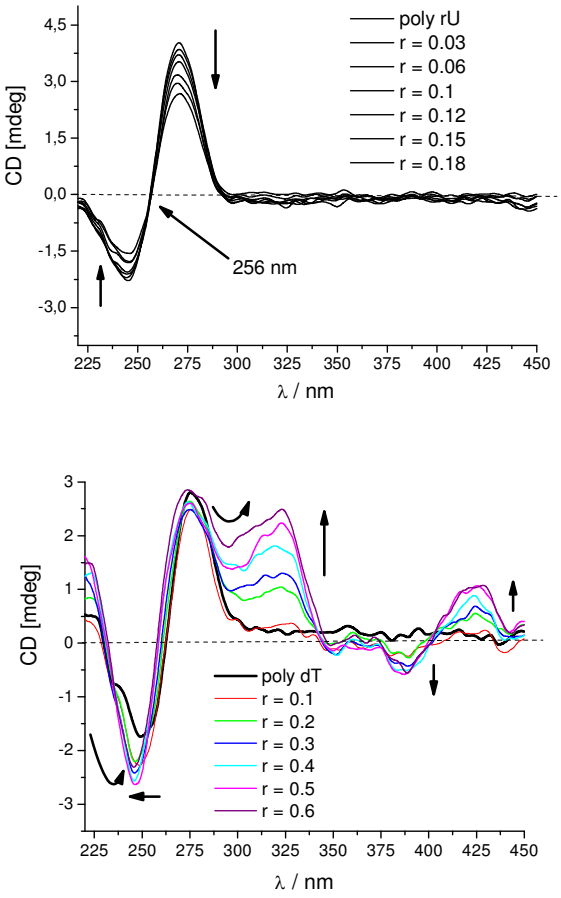

Fig. 2 Changes in CD spectra of poly rU (up) and poly dT (down); c(polynucleotide) = 3.0 × 10^{-5} mol dm^{-3} upon titration with **1**. Done at pH=7, sodium cacodylate buffer, I = 0.05 mol dm^{-3}.

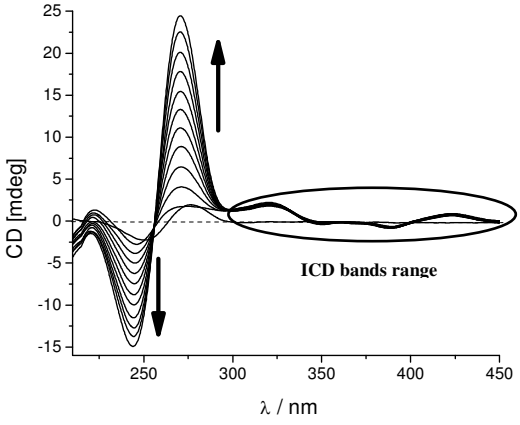

Fig. 3 Changes in the CD spectra of **1**/poly dT complex (*c*(poly dT) = 1.5 × 10^{-5} mol dm^{-3}; *c*(**1**)= 7.5 × 10^{-6} mol dm^{-3}), upon addition of an 1-10fold excess of poly U (ratio = [poly U] / [poly dT]). Done at pH 7.0, buffer sodium cacodylate, *I* = 0.05 mol dm^{-3}. Increase of CD bands intensity at 245 nm and 275 nm corresponds to the CD spectrum of free poly rU.

Competitive experiment performed by adding up to 10-fold excess of poly U (Figure 3) or other ss-DNA/RNA to the **1**/poly dT complex did not result in decrease of the characteristic ICD bands (300 – 450 nm range), thus additionally supporting the affinity preference shown in binding constants (Table 1).

The ^{1}H NMR experiments on **1** performed with both poly dT and oligo dT_{10} revealed strong broadening and pronounced decrease of **1** proton signals upon complex formation (not shown), which can be attributed to involvement of **1** in intensive aromatic stacking interactions, possibly combined with additional aggregation of several complexed systems (due to order of magnitude higher concentrations of **1** in NMR experiments (**1** in 0.05 mM and oligo dT 0.1 mM concentration) in comparison to previously described spectrophotometric methods). However, resulting weak and very broad proton signals were unsuitable for efficient NOE experiments, hampering the determination of intramolecular contacts in **1**/oligo dT_{10}.

Molecular modelling

The most intriguing result was up until know unmatched property of **1** to bind significantly stronger to poly dT than to poly rU and give specific chirooptical signal for poly dT. To shed more light on this recognition process, we addressed the **1**/dT and **1**/rU complexes by molecular modelling. Analysis started from the same geometry: DBTAA moiety was inserted between adjacent nucleobases (supported by UV/vis and ICD results), adenine forming H-bonds with rU or dT (ESI†, Fig. S17 and S18). The complexes were solvated, energy optimized, and subjected to MD simulations. The complex between poly dT and **3** was built from the **1**-poly dT complex by removing adenine. The initial aromatic stacking between DBTAA and nucleobases of the complexes was not disrupted during the 3 ns of MD simulations at room temperature.

Results pointed to the pronounced difference between the final structures of the **1**/dT and **1**/rU complexes. Namely, in the **1**/dT complex (Fig. 4) intramolecular stacking between adenine and DBTAA is preserved (imidazole ring to DBTAA-double bond distance 3.36 Å) and adenine with one of the *o*-xylyl linkers is at the 3.6-4 Å distance (angle of about 45^{0}), suggesting either edge-to-face or face-to-face aromatic stacking interactions. Also, adenine forms two H-bonds with thymine, latter stacked above benzene of DBTAA at 3.81 Å. The thymines at the top and the bottom of the structure are stacked to adjacent thymines by distance of 3.34 Å and 3.62 Å, respectively. From the viewpoint along phosphate backbone axis, sequence T-T-DBTAA-T-T formed helical structure. Moreover, the thymine methyl is positioned above the centre of pyridyl- of **1** (distance 2.8 Å), suggesting the existence of the CH - π interaction. Such binding motif of **1** can be repeated along poly dT forcing the thymidines into intensively stacked, helical structure, which is clearly better organized than the intrinsic structure of the free poly dT.[14] Therefore, evident aromatic stacking of DBTAA moiety between two thymines in well-ordered structure of the **1**/poly dT complex (Fig. 4) controlled the uniform orientation of DBTAA chromophore transition moments in respect to chiral axis of newly formed helical structure, which in turn can explain the induced ICD bands above 300 nm, characteristic for DBTAA moiety.[12,13]

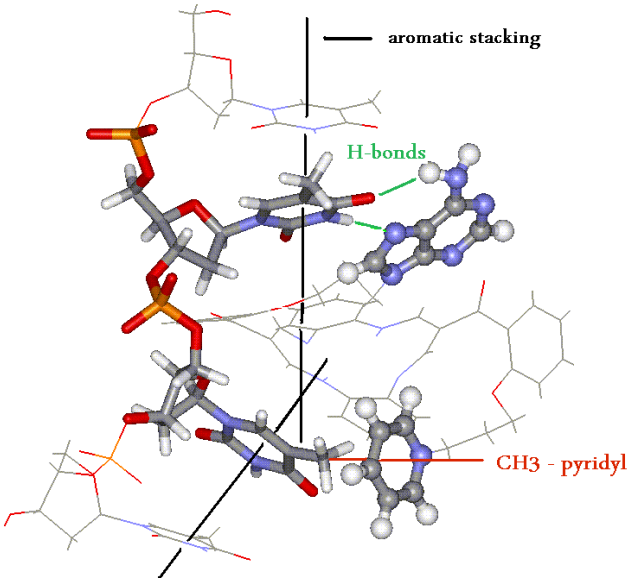

Fig. 4 Structure of a **1**/poly dT complex obtained by molecular modeling. Black lines mark the aromatic stacking interactions between thymines and DBTAA, green lines denote H-bonds between adenine and thymine, red line marks interaction between dT-methyl with pyridyl- of **1**.

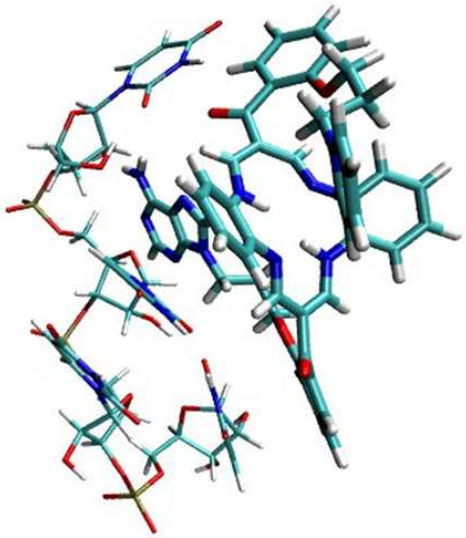

Fig. 5 Structure of a **1**/poly rU complex obtained by molecular modeling. Note stacking of only one uracil with DBTAA and disruption of stacking between uracils along poly rU helical axis.

The structure of the **1**/ poly rU complex obtained by modelling from the same starting point as previous dT-version (Fig. 5) is stabilized mostly by aromatic stacking interactions between various uracils with DBTAA phenyl (3.37 Å), and *o*-xylyl linkers (3.87 Å and 3.81 Å). Furthermore, adenine is edge-to-face oriented pointing proton H8 to the centre of DBTAA (3.7 Å). Hydrogen bonds between adenine (of **1**) and uracil are missing and uracil does not have methyl to form interaction with pyridyl- of **1**, instead, the pyridyl- is stacked to the phenyl-DBTAA (3.7 Å). The structural outcome is oligo rU severely kinked around molecule of **1**, whereby the

stacking between uracils is completely lost. Such a binding mode of **1** disrupts even more intrinsically poorly organised poly rU structure, which decreases the intensity of already weak CD bands of poly rU. Consequently, absence of significant chiral helicity of polynucleotide/**1** complex completely failed to induce any ICD band above 300 nm.

Application of the identical modelling approach to reference compound **3** yielded completely different structure of the **3**/poly dT complex.[†] Compound **3** does not have adenine to form H-bonds with thymine and also the interaction between dT-methyl and **3**-pyridyl was missing. Such poorly organized complex is not likely to give uniform organization of DBTAA units and thus no ICD bands were observed.

Conclusions

Here presented DBTAA-propyl-adenine conjugate **1** was to the best of our knowledge the first small molecule able to selectively recognize ss-dT sequence in respect to the other homogenous ss-DNA/RNA (including rU) by both, strongly increased affinity and specific spectroscopic (ICD) signal. Such selectivity of **1** is exceptionally intriguing because, both, rU and dT can form the same set of hydrogen bonds with adenine (this factor probably excluded poly rC), and both ss-polynucleotides are characterized by similar, poorly organized secondary structure,[14] thus differing only by C5-methyl group specific for thymine and one additional sugar 2'-OH group of rU, respectively. Intriguingly, in analogous double stranded polynucleotide systems the thymine-methyl has also an important role in double stranded helix stabilisation. For instance, poly(dA) - poly(dT) has 50% greater stability than poly(dA) - poly(dU) as a result of the dT-methyl impact[15]. Furthermore, study of the significant differences in stability of DNA *vs.* RNA double stranded helices revealed that contribution of dTC-5 methyl groups is always stabilizing, while 2'-OH groups (present only in RNA) can be stabilizing but also destabilizing, depending on the type of complex.[16] Thus, taking into account an estimation of C5-methyl group contribution to ds-DNA stabilisation of about 0.3 kcal/mol per AT pair[17], combined with the absence of 2'-OH group in poly dT (which increases adjustability of polynucleotide), can explain more efficient adjustment of **1** upon binding to poly dT in comparison to poly rU. That is in accordance with here presented molecular modelling results, showing that the main factors regulating **1**-poly dT selectivity are a) self-stacked DBTAA-adenine system, which is favoured only by short linker of **1** but completely lost for longer linker of **2**, b) H-bonding between adenine and thymine (not present in **1**/poly rU complex and reference compound **3**); c) interaction between thymine-methyl and pyridyl- of **1** (not present in model of **1**/poly rU).

Presented results will have high practical importance in supramolecular design of novel small molecules targeting dT-based sequences, either for ss-DNA or ds-DNA based supramolecular constructs[5] or in biological applications; for instance marking of the oligo (dT)-cellulose commonly used for tRNA purification[18], or T-T sequences which are aside guanine-sequences the most sensitive to radical-induced damage[19]. Furthermore, compounds **1**-**4** are azamacrocyclic ligands and thus have additional potential to bind metal cations,[20] such metal complexes offering a variety of different interactions with DNA/RNA. Preliminary experiments with **4** and several metal cations of biological interest (e.g. Zn^{2+}, Cu^{2+}, La^{3+}) revealed surprisingly low stability of complexes under biologically relevant conditions ($Ks < 10^{-4}$ M^{-1}). Ongoing experiments try to address that issue by design of novel compounds with biologically relevant stability of metal complexes.

Experimental

Synthetic procedures

(7-{2-[3-(aden-9-yl)propoxy]benzoyl}-16-{2-[3-(N-pyridinium-1-yl)propoxy]benzoyl}-5,14-dihydrodibenzo[b,i][1,4,8,11] tetraazacyclotetradecine bromide) (1)

A mixture consisting of adenine (0.266 g, 1.973 mmol), 60% NaH (0.059 g, 1.408 mmol) in anhydrous DMF (5 mL) was stirred for 1 h at room temperature. Compound a (0.76 g, 0.986 mmol) dissolved in anhydrous DMF (60 mL) was added and the reaction mixture was stirred at 40 °C for 5 min, then for 3h at room temperature. The reaction mixture was then transferred to a separatory funnel and partitioned between dichloromethane (150 mL) and water (100 mL). An organic layer was separated, washed with water (2×100 mL), dried over anhydrous magnesium sulfate, concentrated to a small volume and chromatographed on a column of silicagel using dichloromethane/methanol (40:2 v/v) as eluent. A main orange fraction was collected and evaporated to dryness. A residue was dissolved in pyridine (6 mL) and stirred C for 9h at 45°. An excess of pyridine was removed under diminished pressure and a residue was chromatographed on a column with basic aluminium oxide, using dichloromethane/methanol (20:3 v/v) as eluent. A main orange fraction was collected, concentrated to a small volume and diluted with n-hexane to precipitate an orange product (0.144 g, 16%).

Mp: 164-166 °C. ^{1}H-NMR (300 MHz, DMSO-d_6, δ): 2.10 (2H, m, H^h), 2.28 (2H, m, H^b), 4.03 (2H, t, J = 6.0 Hz, H^g), 4.12 (4H, m, H^a, H^i), 4.65 (2H, t, J = 6.9 Hz, H^c), 7.04 (2H, s, H^o), 7.08-7.24 (12H, m, H^1-H^4, H^{12}-H^{15}, H^{26}, $H^{26'}$, H^{28}, $H^{28'}$), 7.35 (2H, m, H^{25}, $H^{25'}$), 7.50 (2H, m, H^{27}, $H^{27'}$), 7.85 (1H, s, H^m), 7.90 (1H, s, H^j), 7.96 (2H, m, H^e), 8.36 (2H, d, J = 6.5 Hz, {H^7, H^9}/{H^{18}, H^{20}}), 8.45-8.52 (3H, m, {H^7, H^9}/{H^{18}, H^{20}}, H^f), 8.98 (2H, m, H^d), 14.20 (2H, m, H^{10}, H^{21}). ^{13}C-NMR (75 MHz, DMSO-d_6, δ): 29.0 (C^h), 30.0 (C^b), 58.3 (C^c), 65.0 (C^a), 65.2 (C^g), 109.8, 110.2 (C^8, C^{19}), 112.7, 113.0 (C^{28}, $C^{28'}$), 115.3, 115.4 (C^1, C^4, C^{12}, C^{15}), 118.7 (C^k), 121.0, 121.1 (C^{26}, $C^{26'}$), 126.7 (C^2, C^3, C^{13}, C^{14}), 127.8 (C^e), 128.6, 128.8 (C^{24}, $C^{24'}$), 129.2 (C^{25}, $C^{25'}$), 131.4, 131.5 (C^{27}, $C^{27'}$), 136.2, 136.3 (C^5, C^{11}, C^{16}, C^{22}), 140.4 (C^j), 144.6 (C^d), 145.4 (C^f), 149.3 (C^l), 152.1 (C^m), 152.4, 152.6 (C^7, C^9, C^{18}, C^{20}), 154.8, 155.1 (C^{29}, $C^{29'}$), 155.7 (C^n), 191.2, 191.4 (C^{23}, $C^{23'}$). IR (ATR) ν_{max} (cm^{-1}): 1254, 1285, 1326, 1414, 1445, 1487, 1557, 1591, 1642, 2876, 2959, 3059, 3203, 3355. MS (ESI) m/z found: 823.6. Calc. for $C_{48}H_{43}N_{10}O_4^+$: 823.35. Anal. found: C, 61.47; H, 4.98; N, 14.71. Calc. for $C_{48}H_{43}N_{10}O_4Br{\cdot}2H_2O$: C, 61.34; H, 5.04; N, 14.90%.

(7-{2-[6-(aden-9-yl)hexoxy]benzoyl}-16-{2-[6-(N-pyridinium-1-yl)hexoxy]benzoyl}-5,14-dihydrodibenzo[b,i][1,4,8,11] tetraazacyclotetradecine bromide) (2)

A reaction mixture consisting of compound c (0.2 g, 0.378 mmol), anhydrous potassium carbonate (0. 104 g, 0.757 mmol) and 9-(6-bromohexyl)adenine (0.056 g, 0.189 mmol) in anhydrous DMF (40 mL) was stirred for 10 h at 65°C. 1,6-Dibromohexane (0.7 mL, 4.54 mmol) and anhydrous potassium carbonate (0.026 g, 0.189 mmol) were then added and stirring was continued for 24 h, at room temperature. The reaction mixture was transferred to a separatory funnel and partitioned between dichloromethane (20 mL) and water (100 mL). A small amount of solid KBr was added to improve separation of the phases. An organic layer was separated and washed thoroughly with water (5× 30 mL), dried over anhydrous magnesium sulfate, concentrated to a small volume and chromatographed on a column of silicagel with use of dichloromethane/methanol, (20:0.4 v/v) as eluent. The second fraction was collected from the two orange ones of highest intensity. It was evaporated to dryness, dissolved in a small volume of chloroform and once more chromatographed on a column of silicagel, using chloroform/methanol (20:0.4 v/v) as eluent. The main fraction was collected, evaporated to dryness and a solid residue was dissolved in pyridine (5 mL). The mixture was stirred for 7 h at 45°C, then pyridine was removed under diminished pressure and a solid residue was chromatographed on a column with basic aluminium oxide, using dichloromethane/methanol (20:2 v/v) as eluent. A main orange fraction was collected and evaporated to dryness. An orange microcrystalline product was obtained by slow evaporation of methylene chloride solution of the crude material (0.042 g, 11%).

Mp: 194-196 °C. ^{1}H-NMR (300 MHz, DMSO-d_6, δ): 0.97-1.28 (8H, m, aliphatic chain), 1.50 (6H, m, aliphatic chain), 1.64 (2H, m, aliphatic chain), 3.86 (2H, t, J = 7 Hz, H^j), 3.95 (4H, m, H^a, H^o), 4.40 (2H, t, J = 7.5 Hz, H^f), 7.03-7.19 (14H, m, H^1-H^4, H^{12}-H^{15}, H^{26}, $H^{26'}$, H^{28}, $H^{28'}$, H^u), 7.34 (2H, m, H^{25}, $H^{25'}$), 7.49 (2H, m, H^{27}, $H^{27'}$), 7.85 (1H, s, H^s), 7.97 (1H, s, H^p), 8.05 (2H, m, H^h), 8.44 (4H, m, H^7, H^9, H^{18}, H^{20}), 8.53 (1H, m, H^i), 8.93 (2H, m, H^g), 14.20 (2H, m, H^{10}, H^{21}). ^{13}C-NMR (75 MHz, DMSO-d_6, δ): 24.8, 24.9, 25.0, 25.6, 28.2, 28.4, 29.1, 30.6 (C^b-C^e, C^k-C^n), 42.5 (C^o), 60.5 (C^f), 67.7, 67.8 (C^a, C^j), 110.1 (C^8, C^{19}), 112.5 (C^{28}, $C^{28'}$), 115.2 (C^1, C^4, C^{12}, C^{15}), 118.7 (C^q), 120.8 (C^{26}, $C^{26'}$), 126.7 (C^2, C^3, C^{13}, C^{14}), 128.0 (C^h), 128.7, 128.7 (C^{24}, $C^{24'}$), 129.4, 129.3 (C^{25}, $C^{25'}$), 131.5, 131.7 (C^{27}, $C^{27'}$), 136.1, 136.1 (C^5, C^{11}, C^{16}, C^{22}), 140.4 (C^p), 144.4 (C^g), 145.4 (C^i), 149.3 (C^r), 152.2 (C^s), 152.5 (C^7, C^9, C^{18}, C^{20}), 155.2, 155.3 (C^{29}, $C^{29'}$), 155.8 (C^t), 191.6 (C^{23}, $C^{23'}$). IR (ATR) ν_{max} (cm^{-1}): 1239, 1290, 1308, 1414, 1447, 1485, 1558, 1585, 1652, 1679, 2875, 2931, 3059, 3116, 3242, 3374. MS (ESI) m/z found 908.3. Calc. for $C_{54}H_{55}N_{10}O_4^+$: 907.44. Anal. found: C, 65.62; H, 5.95; N, 14.05 . Calc. for $C_{54}H_{55}N_{10}O_4Br$: C, 65.65; H, 5.61; N, 14.18%.

(7-(2-hexoxybenzoyl)-16-{2-[3-(N-pyridinium-1-yl)propoxy]benzoyl}-5,14-dihydrodibenzo[b,i] [1,4,8,11] tetraazacyclotetradecine bromide) (3)

A reaction mixture consisting of compound c (1 g, 1.892 mmol), 1-bromohexane (0.319 mL, 2.27 mmol), anhydrous potassium carbonate (0.313 g, 2.27 mmol) in anhydrous DMF (130 mL) was stirred at 60°C, for 3 h. The mixture was cooled down, transferred to a separatory funnel and partitioned between chloroform(150 mL) and water (200 mL). A few drops of hydrobromic acid solution was added to improve separation of the phases. An organic layer was separated and washed thoroughly with water (7×100 mL), dried over anhydrous magnesium sulfate and evaporated to dryness. A solid residue was dried at 55 °C in vacuo and added to a reaction mixture consisting of 1,3-dibromopropane (1.92 mL, 18.92 mmol), anhydrous potassium carbonate (0.523 g, 3.784 mmol) in anhydrous DMF (30 mL). The mixture was stirred at room temperature for 24 h, then transferred to separatory funnel and partitioned between toluene (100 mL) and water (250 mL). A small amount of solid KBr was added to improve separation of the phases. An organic layer was separated, washed with water (7×100 mL) and dried over anhydrous magnesium sulfate. The solvent was evaporated; a residue was dissolved in a small amount of methanol and left in a refrigerator for 12 h. A solid orange material was filtered off, washed with methanol and dried. It was then chromatographed twice on a column of silicagel using toluene/acetone (40:1 v/v) as eluent. A second orange fraction was collected, evaporated to dryness, dried in vacuo and dissolved in pyridine (4 mL). The mixture was stirred for 3 h at 60°C. An excess of pyridine was evaporated and a solid residue was chromatographed on a column of silicagel using dichloromethane/methanol (10:1 v/v) as eluent. The solvents were evaporated and a residue was dried in vacuo to give an orange-red product (0.065 g, 4%).

Mp: 126-129 °C. ^{1}H-NMR (600 MHz, DMSO-d_6, δ): 0.56 (3H, t, J = 7.1 Hz, H^l), 0.98 (4H, m, H^j, H^k), 1.16 (2H, m, H^i), 1.48 (2H, m, H^h), 2.29 (2H, m, H^b), 3.96 (2H, t, J = 6.0 Hz, H^g), 4.12 (2H, t, J = 6.0 Hz, H^a), 4.65 (2H, t, J = 7 Hz, H^c), 7.07-7.19 (8H, m, H^2, H^3, H^{13}, H^{14}, H^{26}, $H^{26'}$, H^{28}, $H^{28'}$), 7.22-7.26 (4H, m, H^1, H^4, H^{12}, H^{15}), 7.34 (2H, m, H^{25}, $H^{25'}$), 7.50 (2H, m, H^{27}, $H^{27'}$), 8.00 (2H, m, H^e), 8.44 (4H, m, H^7, H^9, H^{18}, H^{20}), 8.53 (1H, m, H^f), 9.00 (2H, m, H^d), 14.22 (1H, t, J = 6.5 Hz, H^{10}/H^{21}), 14.27 (1H, t, J = 6.5 Hz, H^{10}/H^{21}). ^{13}C-NMR (75 MHz, DMSO-d_6, δ): 13.5 (C^l), 21.8, 25.1, 28.5, 30.1, 30.8 (C^b, C^h-C^k), 58.2 (C^c), 65.0, 67.8 (C^a, C^g), 110.0, 110.1 (C^8, C^{19}), 112.4, 113.1 (C^{28}, $C^{28'}$), 115.2, 115.4 (C^1, C^4, C^{12}, C^{15}), 120.8, 121.1 (C^{26}, $C^{26'}$), 126.7, 126.8 (C^2, C^3, C^{13}, C^{14}), 127.9 (C^e), 128.7, 128.7 (C^{24}, $C^{24'}$), 129.0, 129.3 (C^{25}, $C^{25'}$), 131.5, 131.6 (C^{27}, $C^{27'}$), 136.2 (C^5, C^{11}, C^{16}, C^{22}), 144.7 (C^d), 145.5 (C^f), 152.3, 152.5 (C^7, C^9, C^{18}, C^{20}), 154.8, 155.2 (C^{29}, $C^{29'}$), 191.3, 191.5 (C^{23}, $C^{23'}$). IR (ATR) ν_{max} (cm^{-1}): 1252, 1286, 1310, 1396, 1418, 1447, 1488, 1559, 1588, 1647, 2859, 2929, 3057, 3394. MS (ESI) m/z found: 732.6. Calc. for $C_{46}H_{46}N_5O_4^+$: 732.35. Anal. found: C, 66.07; H, 5.73; N, 8.25. Calc. for $C_{46}H_{46}N_5O_4Br \cdot 1.3H_2O$: C, 66.07; H, 5.86; N, 8.37%.

Materials and methods

Elemental analyses were performed on an Elementar vario MICRO cube analyser. 1H and 13C NMR were run on a Bruker AVANCE II 300 and Bruker AVANCE III 600

spectrometers. Chemical shifts (δ) are expressed in parts per million and J values in hertz. Assignments of the NMR signals (for numeration of C-atoms and H-atoms see Scheme 2) were based on H-H COSY, HMBC and HSQC experiments, and literature data.[21] The H-2 and H-8 signals of adenine were differentiated using known method involving deuteration experiments.[11b] ESI mass spectra were taken on a Bruker Esquire 3000 spectrometer. The IR spectra were recorded with a Thermo Fisher Scientific Nicolet IR200. Melting points were measured with use of a Boethius apparatus and were uncorrected.

The UV/vis spectra were recorded on a Varian Cary 100 Bio spectrophotometer and CD spectra on JASCO J815 spectrophotometer at 25°C using appropriate 1cm path quartz cuvettes. For study of interactions with DNA and RNA, aqueous solutions of compounds buffered to pH 7.0 (buffer sodium cacodylate, I=0.05 moldm^{-3}) were used.

Polynucleotides were purchased as noted: poly dA, poly rA, poly rG, poly rC, poly rU, poly dT, oligo dT_{10} (Sigma), calf thymus (ct)-DNA (Aldrich). Polynucleotides were dissolved in Na-cacodylate buffer, I=0.05 mol dm^{-3}, pH 7.0. The calf thymus ctDNA was additionally sonicated and filtered through a 0.45 mm filter.[22] Polynucleotide concentration was determined spectroscopically as the concentration of phosphates. Spectrophotometric titrations were performed and pH 7.0 (I=0.05 mol dm^{-3}, buffer sodium cacodylate) by adding portions of polynucleotide solution into the solution of the studied compound for UV/vis and for CD experiments were done by adding portions of compound stock solution into the solution of polynucleotide. Titration data were processed by Scatchard equation[23] Values for K_s and n given in Table 1 all have satisfactory correlation coefficients (>0.999). Thermal melting curves for DNA, RNA and their complexes with studied compounds were determined as previously described[24,25] by following the absorption change at 260 nm as a function of temperature. Absorbance of the ligands was subtracted from every curve and the absorbance scale was normalized. T_m values are the midpoints of the transition curves determined from the maximum of the first derivative and checked graphically by the tangent method.[24] The ΔT_m values were calculated subtracting T_m of the free nucleic acid from T_m of the complex. Every ΔT_m value here reported was the average of at least two measurements. The error in ΔT_m is ±0.5°C.

Viscometry measurements were conducted with an Ubbelohde viscometer system AVS 370 (Schott). The temperature was maintained at 25 +/- 0.1 °C. Aliquots of drug stock solutions were added to 3.0 ml of 5×10^{-4} mol dm^{-3} ct-DNA solution in sodium cacodylate buffer, I = 0.05 mol dm^{-3}, pH 7.0, with a compound to DNA phosphate ratio r less than 0.2. Dilution never exceeded 4% and was corrected for in the calculations. The flow times were measured at least five times optically with a deviation of ± 0.2 s. The viscosity index α was obtained from the flow times at varying r according to the following equation (1):[26]

(1) $L/L_0 = [(t_r - t_0) / (t_{polynucleotide} - t_0)]^{1/3} = 1 + \alpha * r$

Where t_0, $t_{polynucleotide}$ and t_r denote the flow times of buffer, free polynucleotide and polynucleotide complex at ratio $r_{[compound] / [polynucleotide]}$, respectively; L/L_0 is the relative DNA/RNA lengthening. The L/L_0 to $r_{[compound] / [polynucleotide]}$ - plot was fitted to a straight line that gave slope α. The error in α is < 0.1.

Agarose gel electrophoresis was performed on a 1% agarose in TAE buffer (pH8), using TAE as a running buffer[27], applying constant voltage of 30V for two hours, followed by quick staining of the gel with EB solution (0.5μg/mL). Supercoiled plasmid DNA (pCI) was treated by compounds **1**-**3** and ethidium bromide as a reference for the intercalation.

Molecular modeling methods. Single stranded tetranucleotides, DNA (poly dT) and RNA (poly rU) were built with the program *nucgen*, a part of the Amber program suit.[28] Compounds **1** and **3** were built using module 'Builder' within program *InsightII*.[29] Complexes with ss-polynucleotides were built by intercalating the aromatic ring of DBTAA into the space between two adjacent bases in the middle of the polynucleotides. The adenine of **1** was oriented in the way form two H-bonds with the polynucleotide-base, (thymine and uracil in the complex with ss-DNA and ss-RNA, respectively).

Parameterization was performed within the AMBER ff99SB force filed of Duan et al.[30] and the general AMBER force field GAFF. Each complex was placed into the centre of the octahedral box filled with TIP3 type water molecules, a water buffer of 7 Å was used, and Na^+ ions were added to neutralize the systems. The solvated complexes were geometry optimized using steepest descent and conjugate gradient methods, 2500 steps of each. The optimized complexes were heated in steps of 100 K, each lasting 200 ps, while the volume was kept constant. The equilibrated systems were subjected to 3 ns of the productive unconstrained molecular dynamics (MD) simulation at constant temperature and pressure (300 K, 1 atm) using Periodic Boundary Conditions (PBC). The time step during the simulation was 1 fs and the temperature was kept constant using Langevin dynamics with a collision frequency of 1 ps^{-1}. The electrostatic interactions were calculated by the Particle Mesh Ewald (PME) method with cutoff-distance of 11 Å for the pairwise interactions in the real space. Geometry optimization and molecular dynamics (MD) simulations were accomplished using the AMBER 9 program package.

Acknowledgments:

Financial support by the Ministry of Science, Education, Sport of Croatia (098-0982914-2918, 098-1191344-2860), the Grant (WCh-BW) Jagiellonian University, Krakow, Poland, European Regional Development Fund, Polish Innovation Economy Operational Program (contract POIG.02.01.00-12-023/08) is acknowledged.

Notes and references

[a] *Division of Organic Chemistry and Biochemistry, Division of Physical Chemistry, NMR Centre, Ruđer Bošković Institute, Bijenička cesta 54, PO Box 180, HR-10002 Zagreb, Croatia, E-mail: pianta@irb.hr*

[b] *Department of Chemistry, Jagiellonian University, Ingardena 3 ,30-060 Kraków, Poland*

† Electronic Supplementary Information (ESI) available: Characterization of **1**-**3**; detailed experiments with DNA and RNA, molecular modelling procedures and additional data. See DOI: /

1 S. Yoshizawa, G. Kawai, K. A. Watanabe, K. I. Miura and I. Hirao, *Biochemistry,* 1997, **36,** 4761.
2 H. Naegeli, in *Mechanism of DNA Damage Recognition in Mammalian Cells*, Springer-Verlag, Heidelberg, Germany, 1997.
3 C. Bailly and M. J. Waring, in *Methods in Molecular Biology*, Vol. 90, Humana Press, Totowa, NJ, 1997, pp. 51-79.
4 a) J. Lhomme, J. F. Constant and M. Demeunynck, *Biopolymers,* 1999, **52**, 65-83; b) A. Martelli, J. F. Constant, M. Demeunynck, J. Lhomme and P. Dumy, *Tetrahedron,* 2002, **58***,* 4291.
5 Y. N.Teo and E. T. Kool, *Chem Rev*, 2012, **112**, 4221.
6 E. Kimura and S. Aoki, *J. Am. Chem. Soc*., 2000, **122,** 4542.
7 B. M. Zeglis, J. A. Boland and J. K. Barton, *J. Am. Chem. Soc*., 2008, **130,** 7530.
8 S. Miura, S. Nishizawa, A. Suzuki, Y. Fujimoto, K. Ono, Q. Gao, and N. Teramae, *Chem. Eur. J.*2012, **17**, 14104.
9 a) L.-M. Tumir, I. Piantanida, I. Juranović, Z. Meić, S. Tomić and M. Žinić, *Chem. Commun*., 2005, 2561; b) I. Juranović, Z. Meić, I. Piantanida, L.-M. Tumir, M. Žinić, *Chem. Commun*., 2002 1432; c) V. Malinovski, L. Tumir, I. Piantanida, M. Žinić and H.-J. Schneider, *Eur. J. Org. Chem*., 2002, **22,** 3785.
10 a) M. Radić Stojković, I. Piantanida, M. Kralj, M. Marjanović, M. Žinić, D. Pawlica and J. Eilmes, *Bioorg. Med. Chem*., 2007, **15,** 1795; b) M. Radić Stojković, M. Marjanović, D. Pawlica, L. Dudek, J. Eilmes, M. Kralj and I. Piantanida, *New J. Chem.,* 2010, **34,** 500; c) D. Pawlica, M. Radić Stojković, Ł. Dudek, I. Piantanida, L. Sieroń and J. Eilmes, *Tetrahedron,* 2009, **65,** 3980.
11 a) I. Sigg, G. Haas, T. Winkler *Helv. Chim. Acta*, 1982, **65**, 275; b) T. Itahara; *J. Chem. Soc., Perkin. Trans*. 2, 1996, 2695.
12 M. Eriksson, B. Norden, *Method Enzymol* 2001, **340**, 68.
13 Nichola C. Garbett, P. A. Ragazzon and J. B. Chaires, *Nat. Prot.* 2007, **2**, 3166
14 C. R. Cantor and P. R. Schimmel, in *Biophysical Chemistry*, Vol. 3., WH Freeman and Co., San Francisco, 1980, pp. 1109-1181.
15 P. D. Ross and F. B. Howard, *Biopolymers* 2003, **68**, 210.
16 S. H. Wang and E. T. Kool, *Biochemistry* 1995, **34**, 4125.
17 T. B. Xia, J. SantaLucia, M. E. Burkard, R. Kierzek, S. J. Schroeder, X. Q. Jiao, C. Cox and D. H. Turner, *Biochemistry* 1998, **37**, 14719.
18 J. Sambrook, E. F. Fritsch and T. Maniatis, in *Molecular Cloning, a laboratory manual*, Vol 1-3, Cold Spring Harbor Laboratory Press, New York, 1989.
19 G. B. Schuster, A. Ghosh, A. Joy, T. Douki and J. Cadet, *Org. Biomol. Chem*., 2008, **6,** 916.
20 K. Lewinski and J. Eilmes, *J. Incl. Phenom. Macro*., 2005, **52**, 261.
21 R. S. Iyer, M. W. Voehler, T. M. Harris, *J. Am. Chem. Soc*., 1994, **116**, 8863.
22 J. B. Chaires, N. Dattagupta and D. M. Crothers, *Biochemistry*, 1982, **21**, 3933.
23 G. Scatchard, *Ann. N.Y. Acad. Sci*., 1949, **51**,660.; J. D. McGhee, P. H. von Hippel, *J. Mol. Biol.,* 1976, **103,** 679.
24 I. Piantanida, B.S. Palm, P. Čudić, M. Žinić, H.-J. Schneider; *Tetrahedron*, 2004,**60**, 6225.
25 J. L. Mergny, L. Lacroix, *Oligonucl.*, 2003, **13,** 515.
26 G. Cohen and H. Eisenberg, *Biopolymers*,1969, **8**, 45; M. Wirth, O. Buchardt, T. Koch, P. E. Nielsen and B. Nordén, *J. Am. Chem. Soc*., 1988, **110**, 932.
27 I. Lubitz, D. Zikich and A. Kotlyar, *Biochemistry* 2010, **49**, 3567.
28 http://amber.scripps.edu/
29 INSIGHTII – Accelerys San Diego 2001-2008; http://accelrys.com/services/training/life-science/insight-migration.html
30 Y. Duan, C. Wu, S. Chowdhury, M.C. Lee, G. Xiong. W. Zhang. R. Yang, P. Cipelak, R. Luo and T. Lee, *J. Comput. Chem*., 2003, **24**, 1999.

Dibenzotetraaza[14]annulene – adenine conjugate recognizes complementary poly dT among ss-DNA / ss-RNA sequences

Marijana Radić Stojković,[a] Marko Škugor,[a] Sanja Tomić,[a] Marina Grabar,[a] Vilko Smrečki,[a] Łukasz Dudek,[b] Jarosław Grolik,[b] Julita Eilmes[b] and Ivo Piantanida*[a]

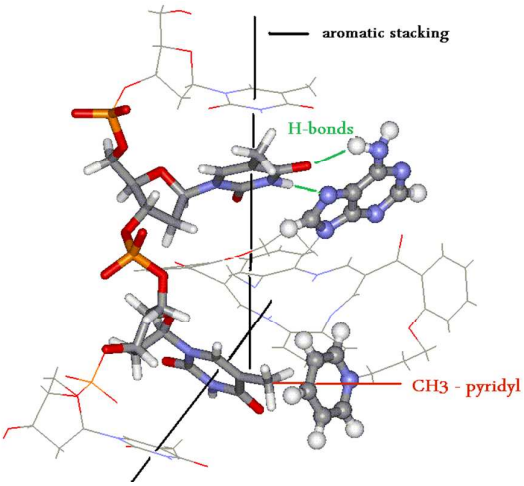

DBTAA-$(CH_2)_3$-adenine: the first small molecule able to recognize consecutive oligo dT sequence by affinity and specific chirooptical (ICD) response

Electronic Supporting Information

Dibenzotetraaza[14]annulene – adenine conjugate recognizes complementary poly dT among ss-DNA / ss-RNA sequences

Marijana Radić Stojković,[a] Marko Škugor,[a] Sanja Tomić,[a] Marina Grabar,[a] Vilko Smrečki,[a] Łukasz Dudek,[b] Jarosław Grolik,[b] Julita Eilmes[b] and Ivo Piantanida*[a]

[a] Division of Organic Chemistry and Biochemistry, Division of Physical Chemistry, NMR Centre, Ruđer Bošković Institute, Bijenička cesta 54, PO Box 180, HR-10002 Zagreb, Croatia, E-mail: pianta@irb.hr
[b] Department of Chemistry, Jagiellonian University, Ingardena 3 ,30-060 Kraków, Poland

SUPPORTING INFORMATION

Contents

1 Additional characterisation data for compounds 1-3:

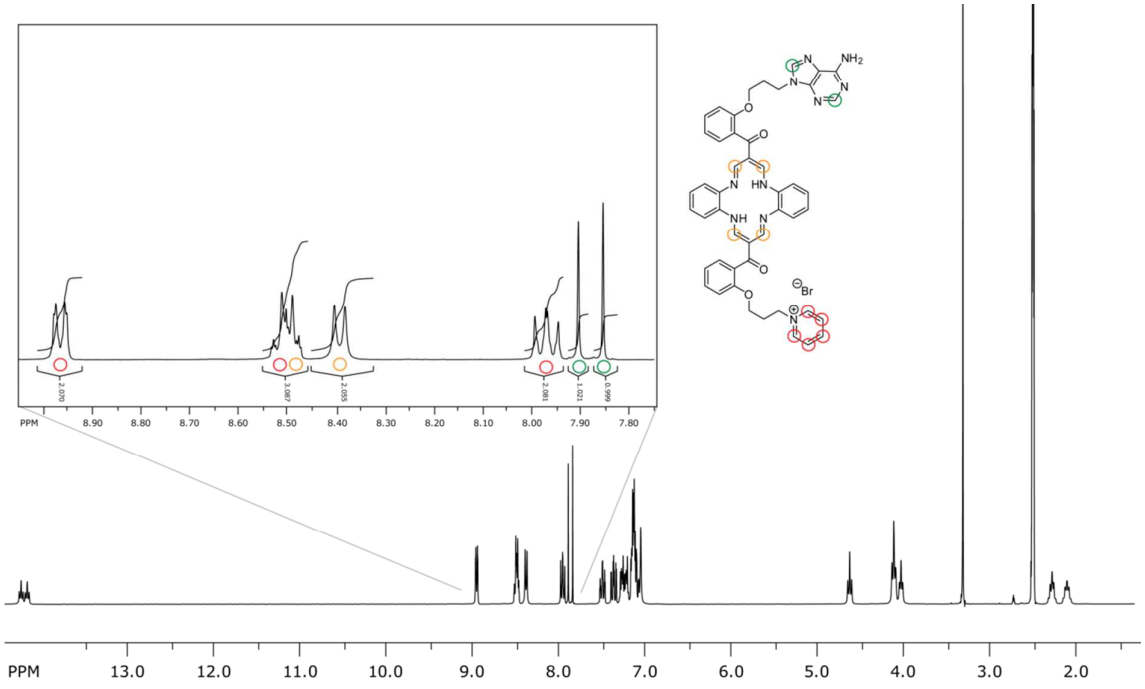

^{1}H-NMR spectrum of **1** in DMSO-d_6

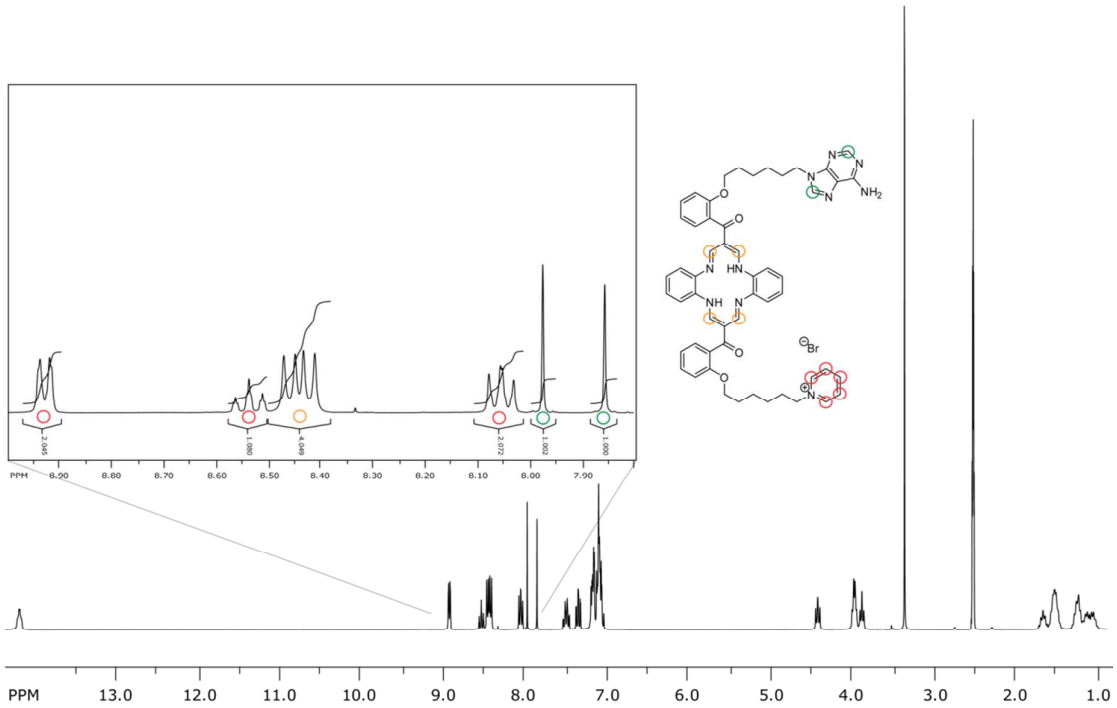

^{1}H-NMR spectrum of **2** in DMSO-d_6

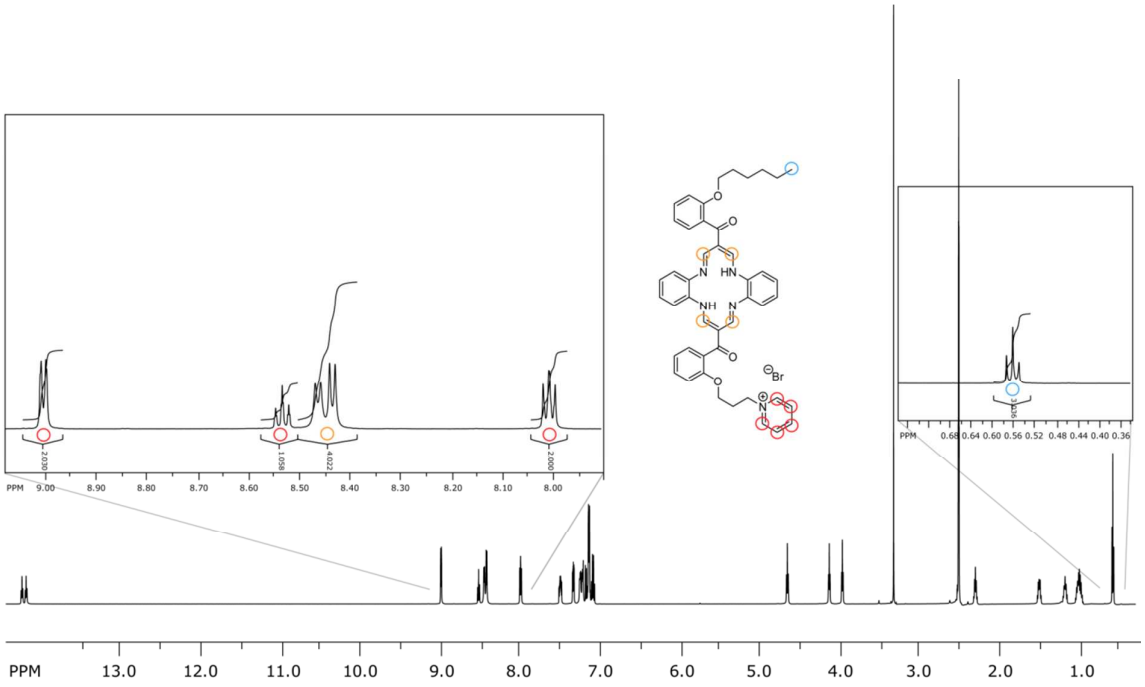

^{1}H-NMR spectrum of **3** in DMSO-d_6

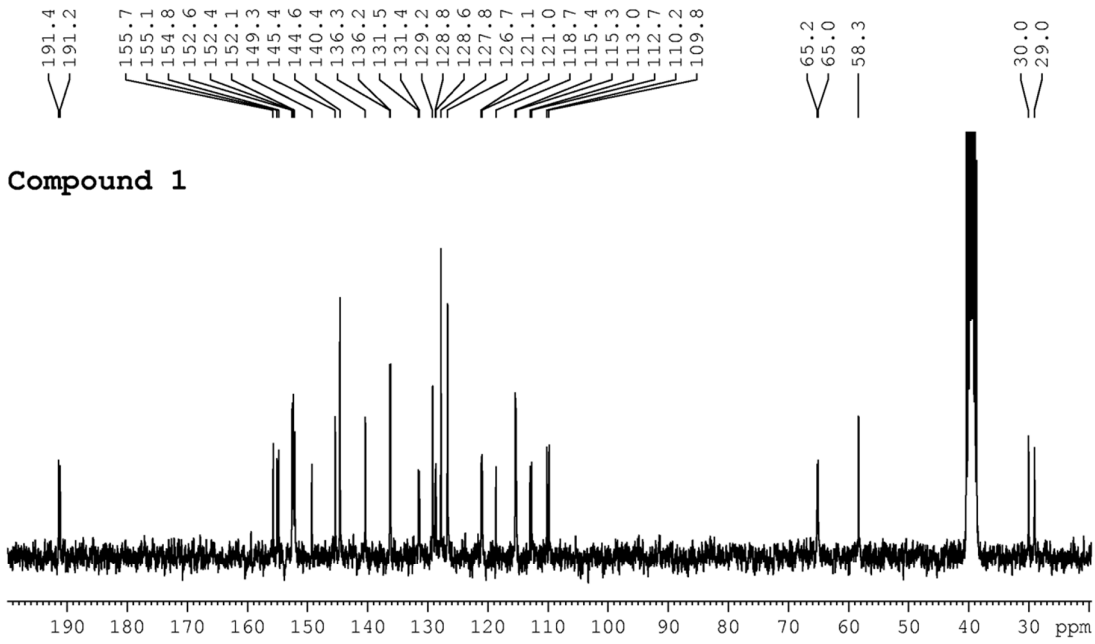

^{13}C-NMR spectrum of **1** in DMSO-d_6

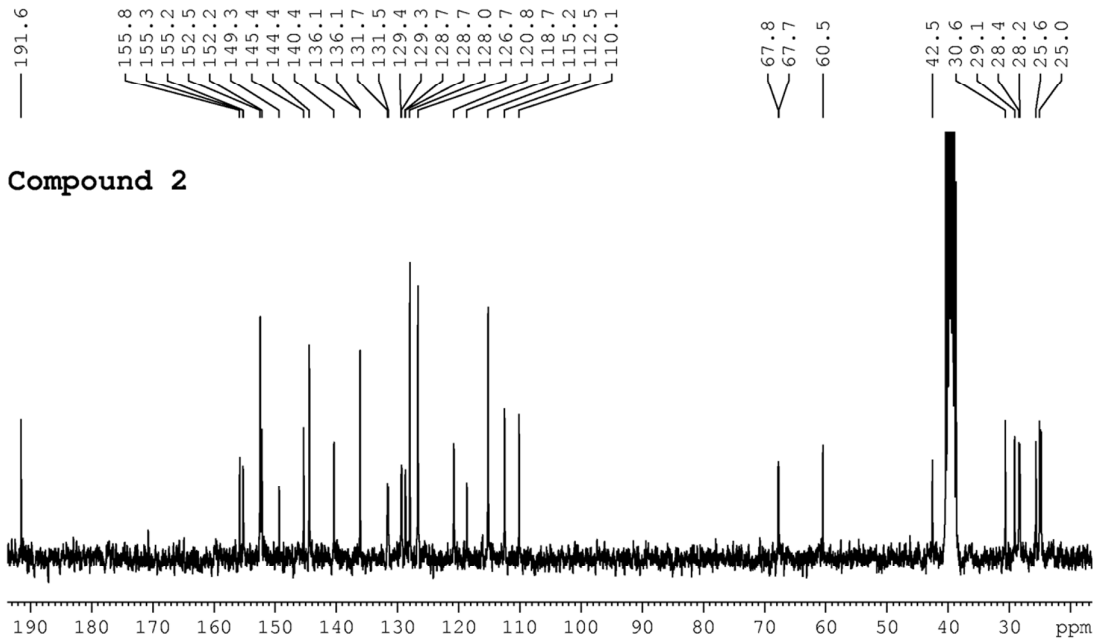

^{13}C-NMR spectrum of **2** in DMSO-d_6

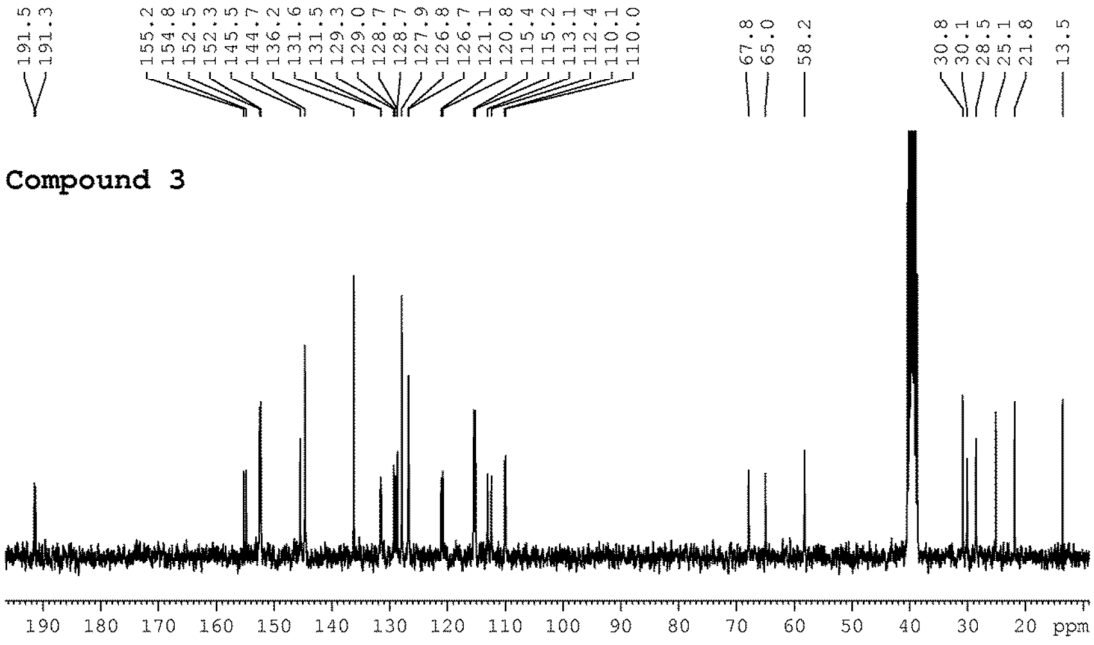

^{13}C-NMR spectrum of **3** in DMSO-d_6

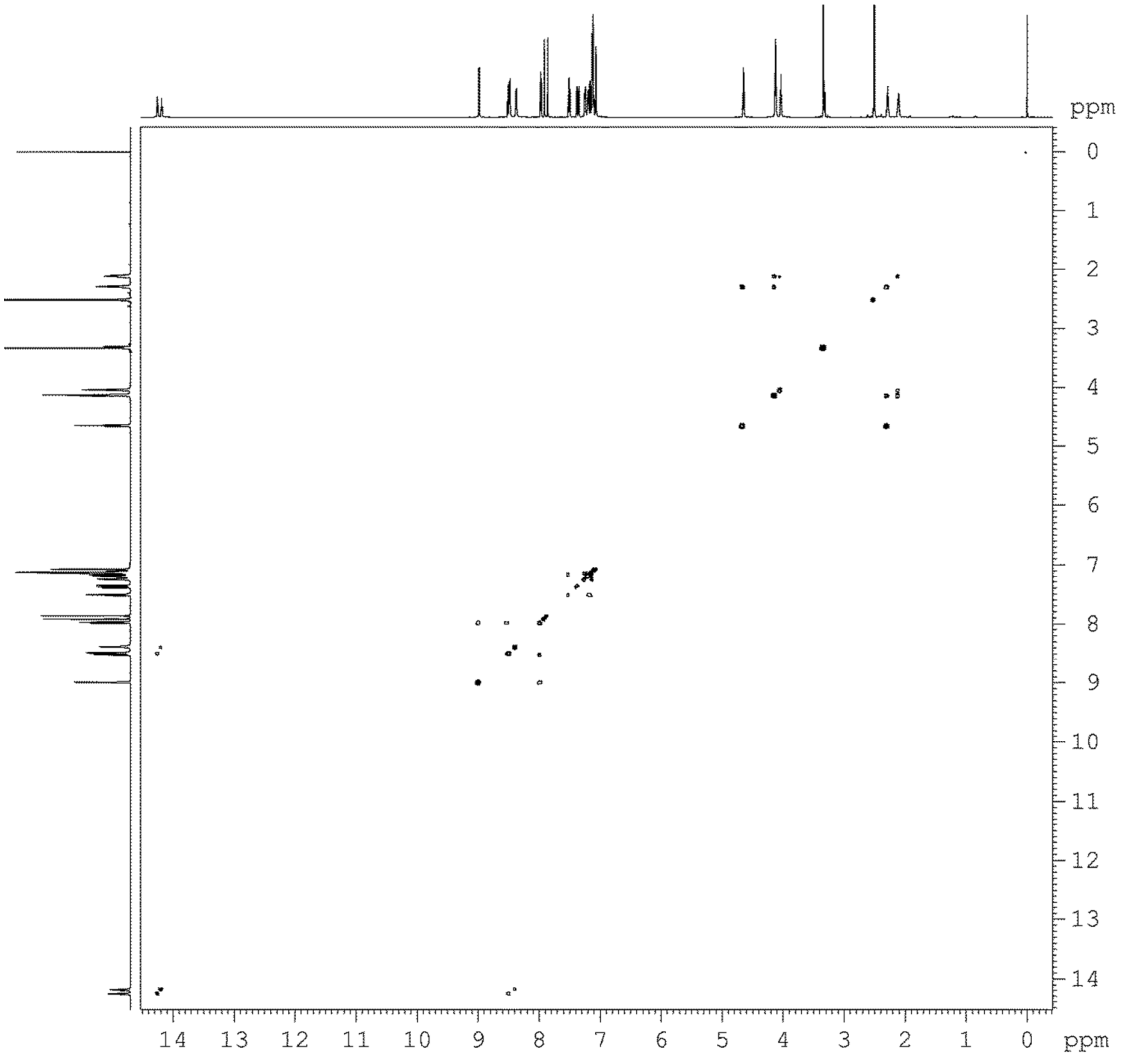

COSY spectrum of **1**

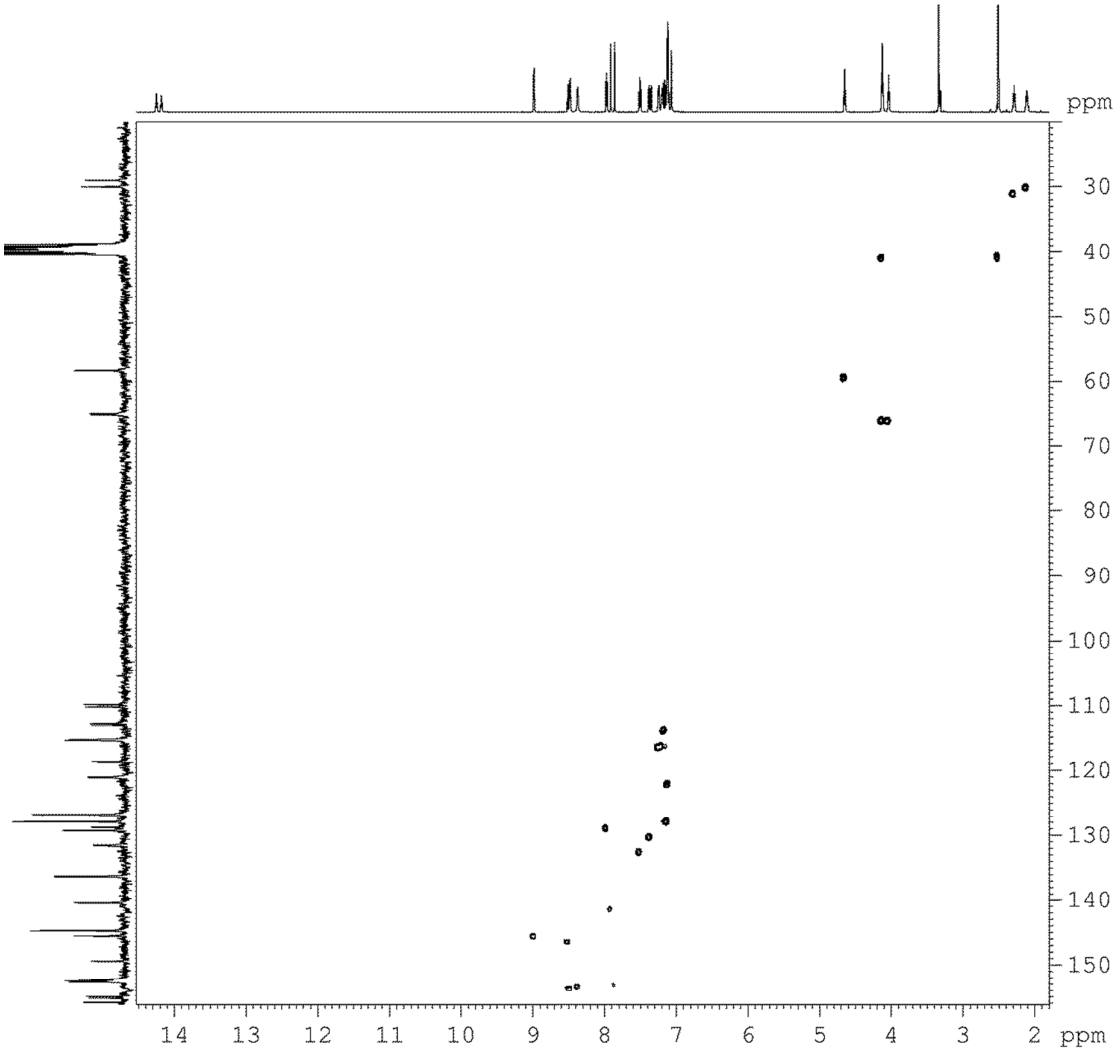

HSQC spectrum of **1**

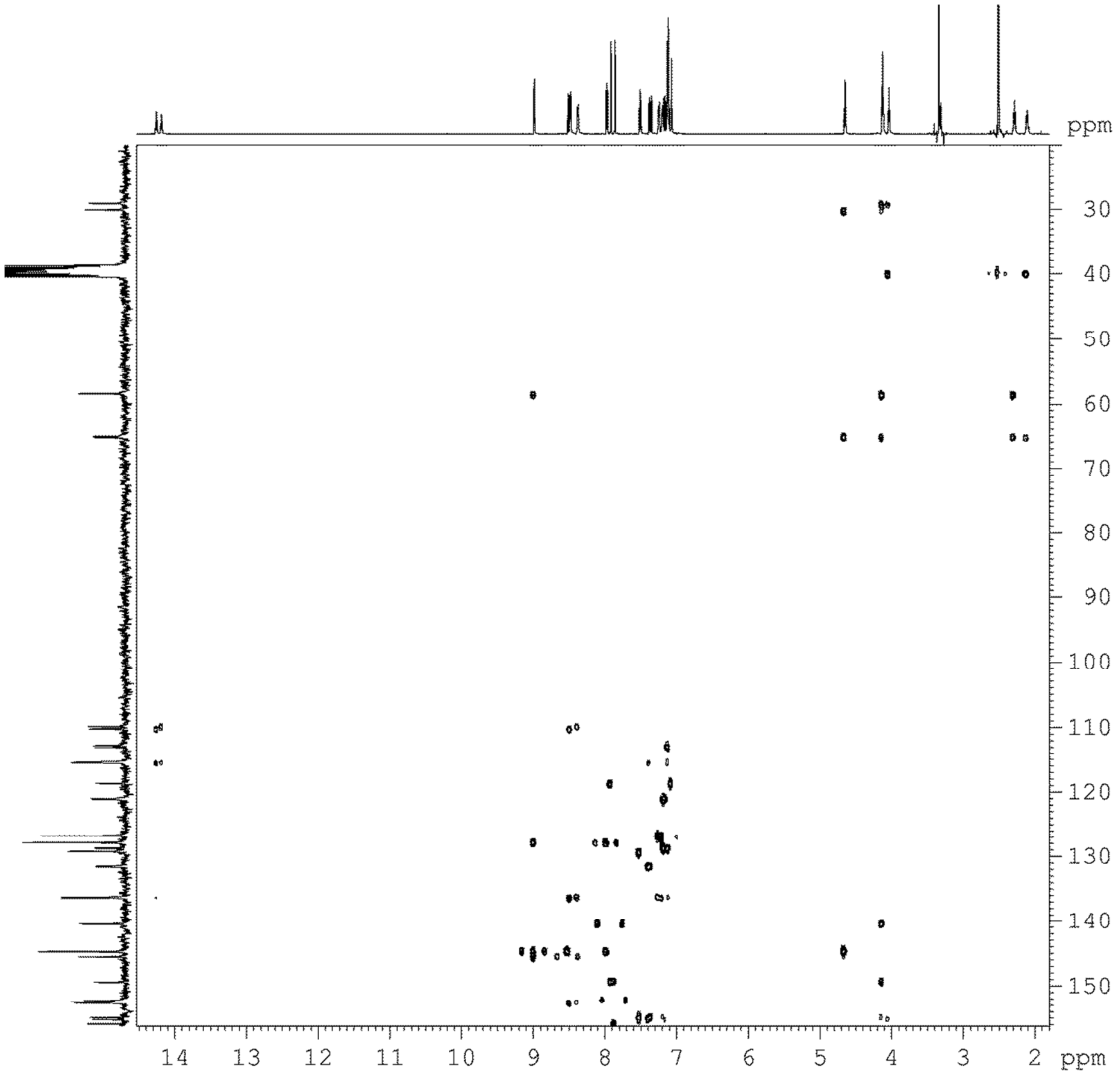

HMBC spectrum of **1**

2 Experimental procedure for Spectroscopy and interactions with DNA/RNA

^{1}H NMR spectra were recorded on Bruker Avance 600 spectrometer (operating at 600.13 MHz for ^{1}H) equipped with TBI probe including z-gradients. Samples in 1 mM sodium cacodylate buffer with 10% D_2O/H_2O were measured at 298 K. Water suppression was achieved using watergate W5 pulse sequence with gradients (from Bruker pulse sequence library). The methyl proton signal of sodium cacodylate buffer was used as internal standard. Proton spectra with spectral width of 12,000 Hz and a digital resolution of 1.4 Hz per point were measured with 128 scans.

Viscometry measurements were conducted with an Ubbelohde viscometer system AVS 370 (Schott). The temperature was maintained at 25 +/- 0.1 °C. Aliquots of drug stock solutions were added to 3.0 ml of 5×10^{-4}mol dm^{-3}ct-DNA solution in sodium cacodylate buffer, I = 0.05 mol dm^{-3}, pH 7.0, with a compound to DNA phosphate ratio r less than 0.2. Dilution never exceeded 4% and was corrected for in the calculations. The flow times were measured at least five times optically with a deviation of ± 0.2 s. The viscosity index α was obtained from the flow times at varying r according to the following equation:[1]

$$L/L_0 = [(t_r - t_0) / (t_{polynucleotide} - t_0)]^{1/3} = 1 + \alpha * r$$

Where t_0, $t_{polynucleotide}$ and t_r denote the flow times of buffer, free polynucleotide and polynucleotide complex at ratio $r_{[compound] / [polynucleotide]}$, respectively; L/L_0 is the relative DNA/RNA lengthening. The L/L_0 to $r_{[compound] / [polynucleotide]}$ -plot was fitted to a straight line that gave slope α. The error in α is < 0.1.

3 Spectroscopy and interactions with DNA/RNA

Table S1. Electronic absorption data of **1, 2, 3**.

	λ_{max} / nm	$\varepsilon \times 10^3$ / mmol^{-1} cm^2	λ_{max} / nm	$\varepsilon \times 10^3$ / mmol^{-1} cm^2
1	256	29.6 ± 0.3	346	37.6 ± 0.2
2	258	32.5 ± 0.3	346	42.1 ± 0.3
3	254	17.8 ± 0.6	342	32.0 ± 0.9

[a] Sodium cacodylate buffer, I = 0.05 mol dm^{-3},pH = 7.0.

The values of molar extinction coefficient (ε) increase with the length of the linker between DBTAA unit and nucleobase, which could be attributed to the weakening of the intramolecular aromatic stacking interactions proportional to the length of the linker.

3.1. Thermal denaturation experiments

It is well known that upon heating ds-helices of polynucleotides at well-defined temperature (Tm value) dissociate into two single stranded polynucleotides. Non-covalent binding of small molecules to ds-polynucleotides usually has certain effect on the thermal stability of helices thus giving different Tm values. Difference between Tm value of free polynucleotide and complex with small molecule (ΔTm value) is important factor in characterization of small molecule / ds-polynucleotide interactions.

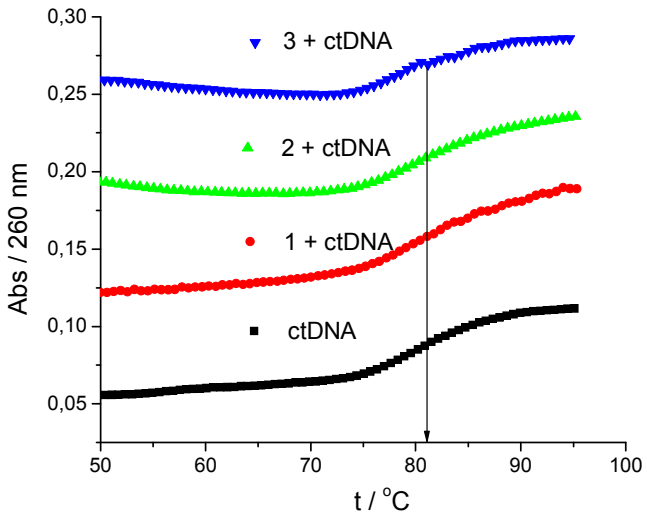

Figure S1. Thermal denaturation curve of **ct-DNA**upon addition of **1** and **2** at $r_{[compound/polynucleotide]}$ = 0.3 and **3** at r = 0.1 (precipitation at higher ratios). Done at pH 7.0 (buffer sodium cacodylate, I = 0.05 mol dm^{-3}).

3.2. Viscometry measurements, CD and gel electrophoresis experiments with ct-DNA

The increase in DNA contour length that accompany an intercalative mode of binding is most conveniently monitored by measuring the viscosity of sonicated rod-like fragments of DNA as a function of ligand binding ratio, r. Cohen and Eisenberg have deduced that the relative increase in contour length in the presence of bound drug is approximated by the cube root of the ratio of the intrinsic viscosity of the DNA-drug complex to that of the free DNA.[1]

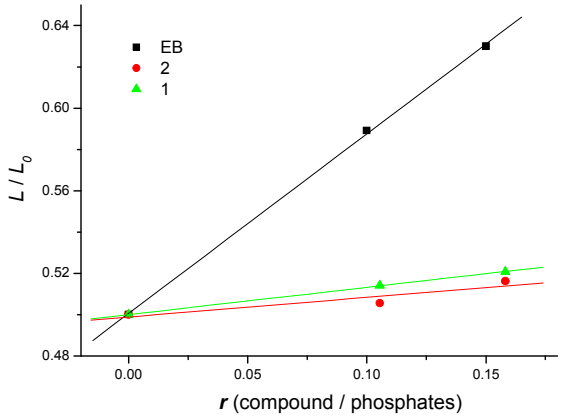

Figure S2. Relative helix length extension of ct-DNA (L/L_0) *vs*. ratio $r_{[compound] / [DNA]}$ plot for **EB**, **1** and **2** at pH 7.0, sodium cacodylate buffer, I = 0.05 mol dm^{-3}.

Viscometry experiments (Figure S2) performed with ct-DNA at pH 7.0 (sodium cacodylate buffer, I = 0.05 mol dm^{-3}) yielded values of α = 0.13 ± 0.01 (**1**), 0.095 ± 0.03 (**2**), and in control experiment for ethidium bromide α(**EB**) = 0.87 ± 0.02. Reference compound **3** precipitated during the experiment.

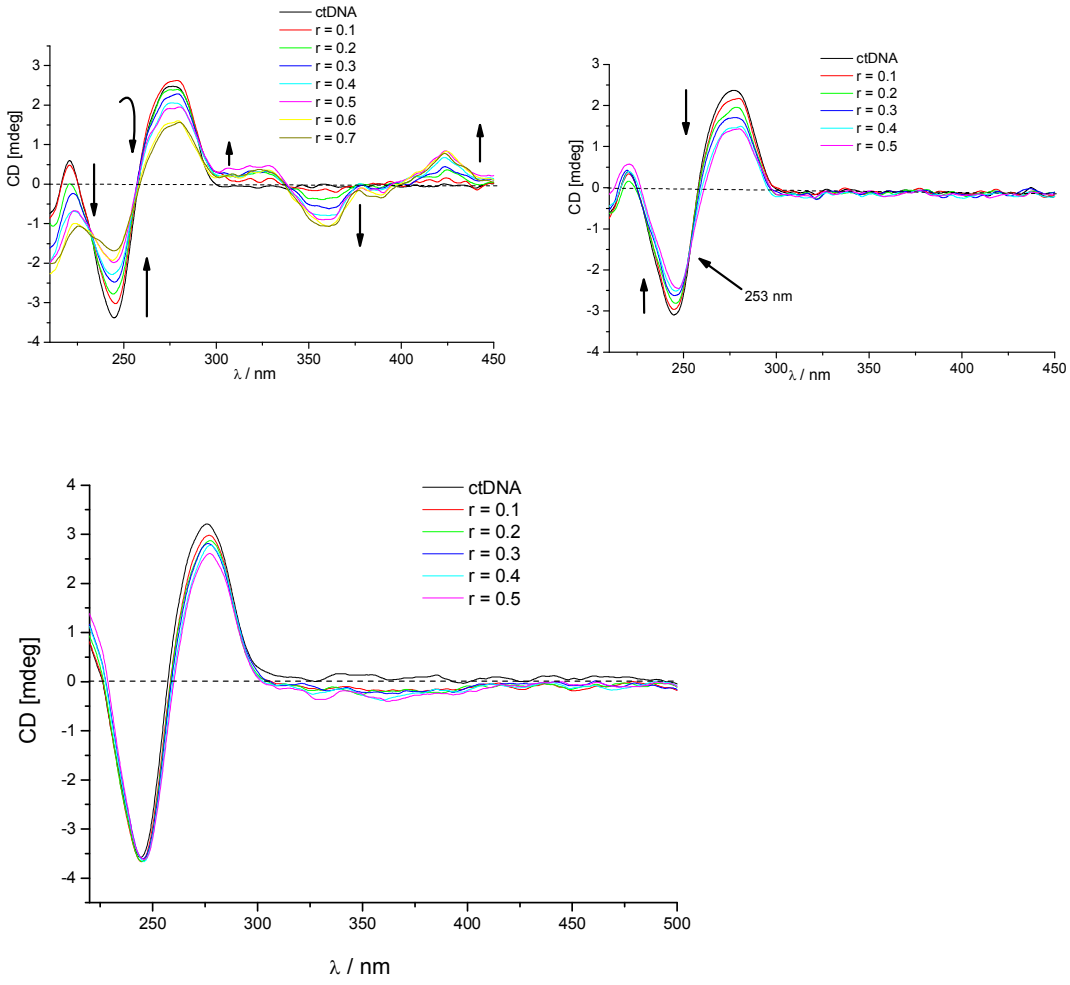

Figure S3. Changes in the CD spectrum of ct-DNA (c = 3.0 × 10^{-5} mol dm^{-3}) upon addition of **1** (left) and **2** (right) and **3** (down) at molar ratios ***r*** = [compound]/ [polynucleotide] (pH 7.0, buffer sodium cacodylate, I = 0.05 mol dm^{-3}).

Agarose gel electrophoresis technique was extensively used for investigating the DNA cleavage efficiency of small molecules and as a useful method to investigate various binding modes of small molecules to supercoiled DNA.[2] Intercalation of small molecules to plasmid DNA can loosen or cleave the SC (*supercoiled*) DNA form, which decreases its mobility rate and can be separately visualized by agarose gel electrophoresis method, whereas simple electrostatic interaction of small molecules to DNA and groove binding does not significantly influence the SC form of plasmid DNA, thus the mobility of supercoiled DNA does not change.[3]

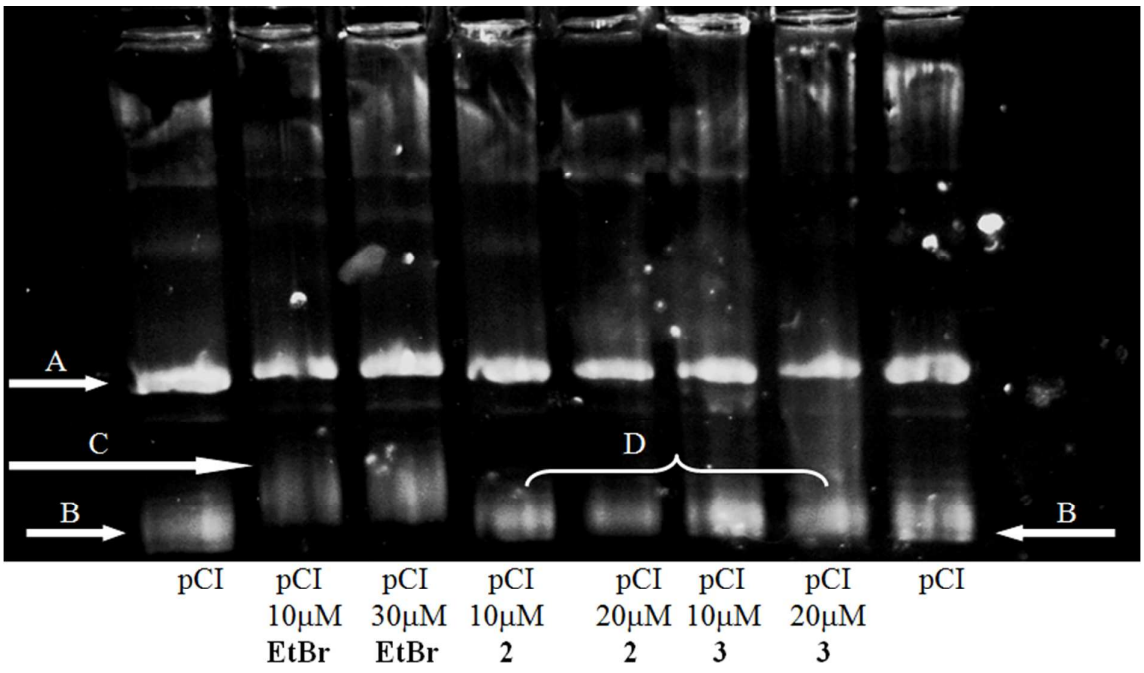

Figure S4. Gel electrophoresis of the supercoiled plasmid DNA, pCI. Arrows point A – open circular plasmid DNA, B – supercoiled circular plasmid DNA, C – supercoiled circular plasmid DNA, retained by intercalated **EB**, D – supercoiled circular plasmid DNA pre-treated with new compounds.

3.3. CD experiments with ss-DNA/RNA

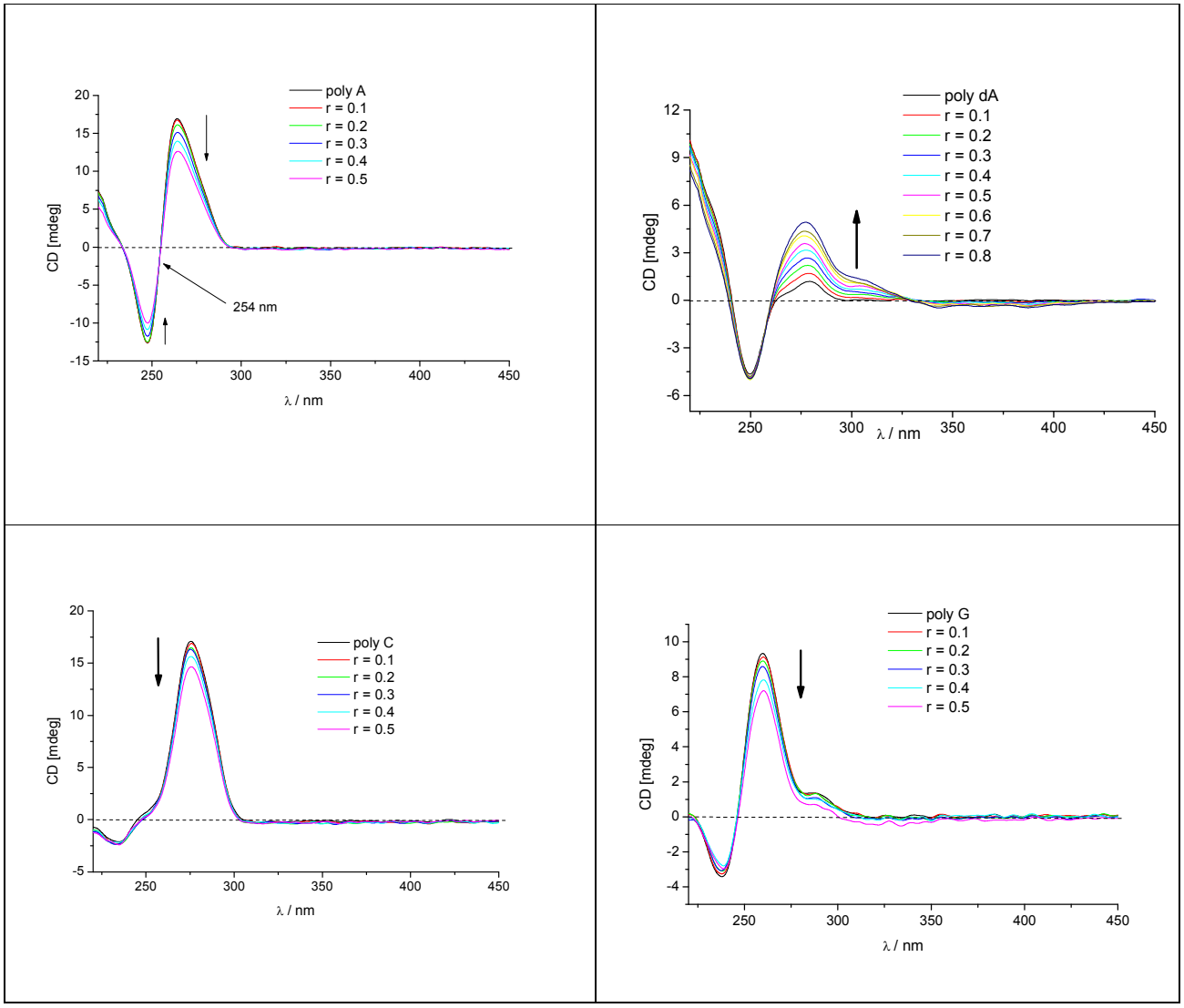

Figure S5. Changes in the CD spectra of ss-polynucleotides (poly A, poly dA, poly C and poly G, c = 3.0 × 10^{-5} mol dm^{-3}), upon addition of **1** at molar ratios ***r*** = [compound]/ [polynucleotide] (pH 7.0, buffer sodium cacodylate, I = 0.05 mol dm^{-3}).

3.4. UV experiments with ss-DNA/RNA

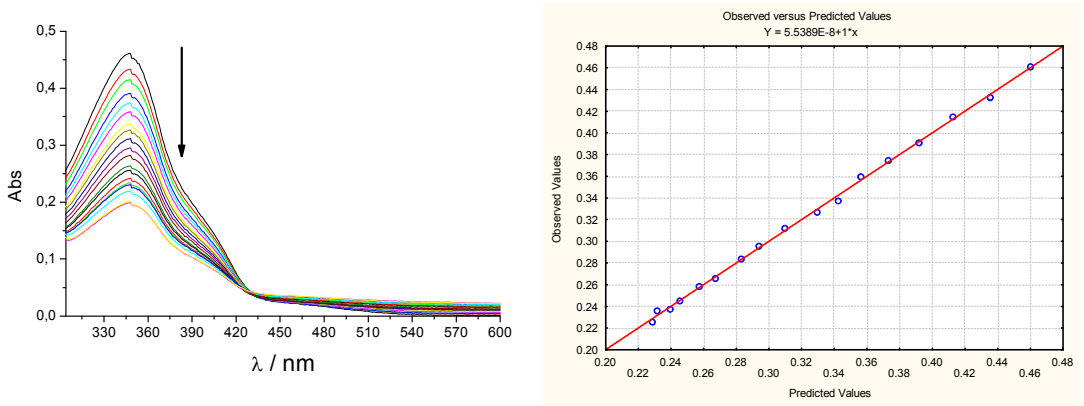

Figure S6. *Left*: Changes in UV/vis spectrum of **1** (c= 1.3 × 10^{-5} mol dm^{-3}) upon titration with poly C (c= 1.7 × 10^{-6} – 1.6 × 10^{-4} mol dm^{-3}); *Right*: Experimental (○) and calculated data (—), processed according to the Scatchard equation, of **1** (λ_{max}=347 nm) as a function of poly C concentration (pH=7, sodium cacodylate buffer, I = 0.05 mol dm^{-3}).

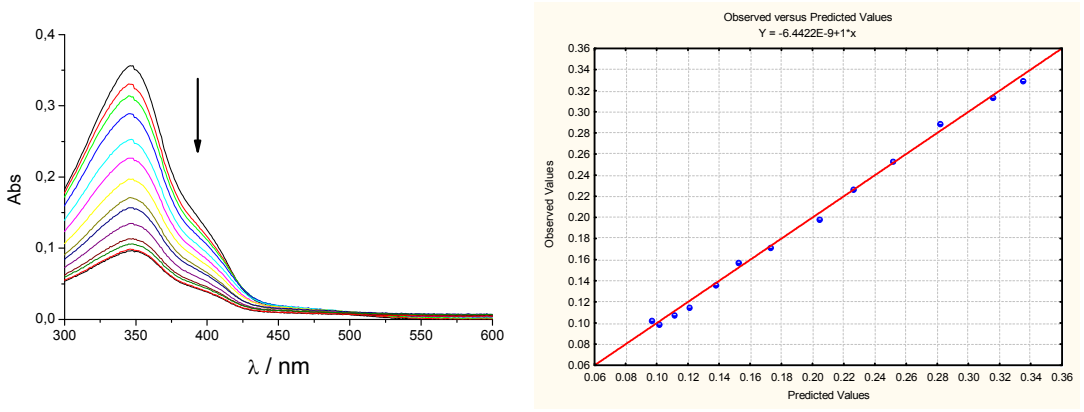

Figure S7. *Left*: Changes in UV/vis spectrum of **1** (c= 1.0 × 10^{-5} mol dm^{-3}) upon titration with poly A (c= 1.9 × 10^{-6} – 1.3 × 10^{-4} mol dm^{-3}); *Right*: Experimental (○) and calculated data (—), processed according to the Scatchard equation, of **1** (λ_{max}=346 nm) as a function of poly A concentration (pH=7, sodium cacodylate buffer, I = 0.05 mol dm^{-3}).

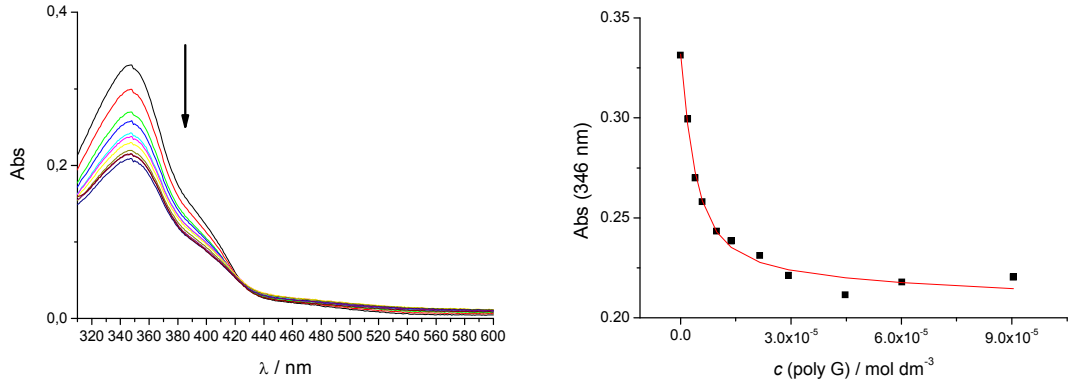

Figure S8. *Left*: Changes in UV/vis spectrum of **1** (c= 1.0 × 10^{-5} mol dm^{-3}) upon titration with poly G (c= 1.9 × 10^{-6} – 9.0 × 10^{-5} mol dm^{-3}); *Right*: Experimental (■) and calculated data (—),

processed according to the Scatchard equation, of **1** (λ_{max}=346 nm) as a function of poly G concentration (pH=7, sodium cacodylate buffer, I = 0.05 mol dm^{-3}).

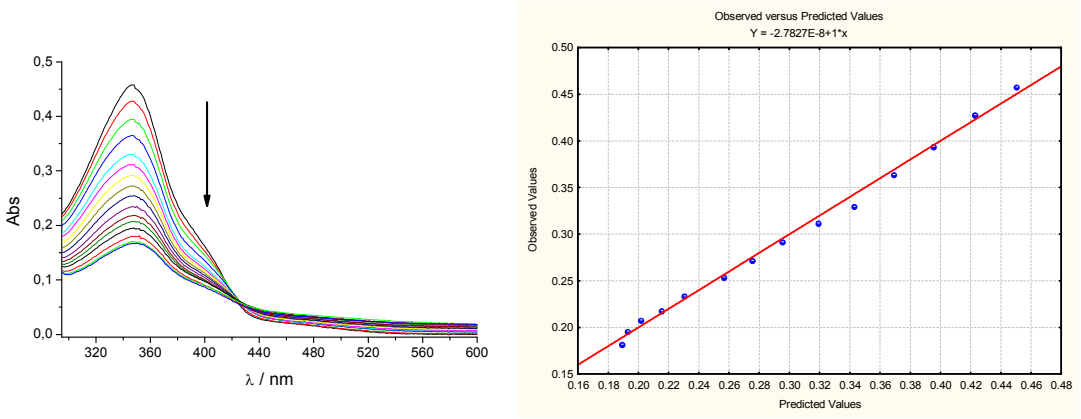

Figure S9. *Left*: Changes in UV/vis spectrum of **1** (c= 1.3 × 10^{-5} mol dm^{-3}) upon titration with poly U (c= 2.8 × 10^{-6} – 1.8 × 10^{-4} mol dm^{-3}); *Right*: Experimental (○) and calculated data (—), processed according to the Scatchard equation, of **1** (λ_{max}=347 nm) as a function of poly U concentration (pH=7, sodium cacodylate buffer, I = 0.05 mol dm^{-3}).

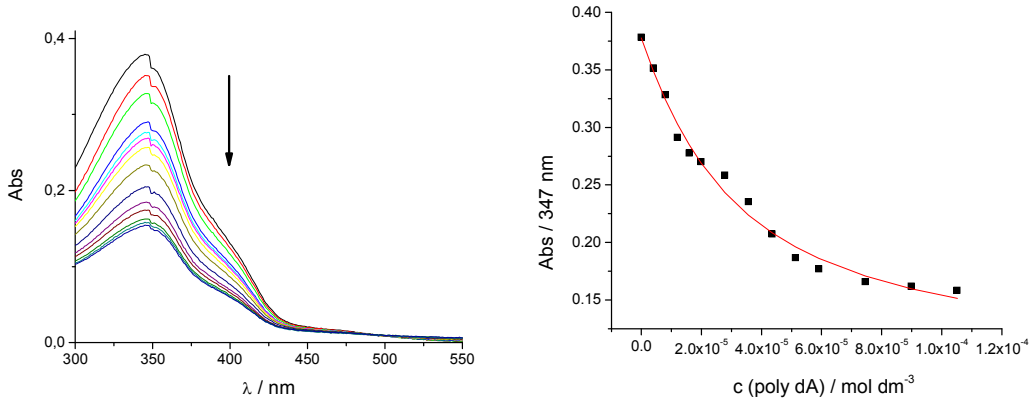

Figure S10. *Left*: Changes in UV/vis spectrum of **1** (c= 9.0 × 10^{-6} mol dm^{-3}) upon titration with poly dA (c= 4.0 × 10^{-6} – 1.0 × 10^{-4} mol dm^{-3}); *Right*: Experimental (■) and calculated data (—), processed according to the Scatchard equation, of **1** (λ_{max}=347 nm) as a function of poly dA concentration (pH=7, sodium cacodylate buffer, I = 0.05 mol dm^{-3}).

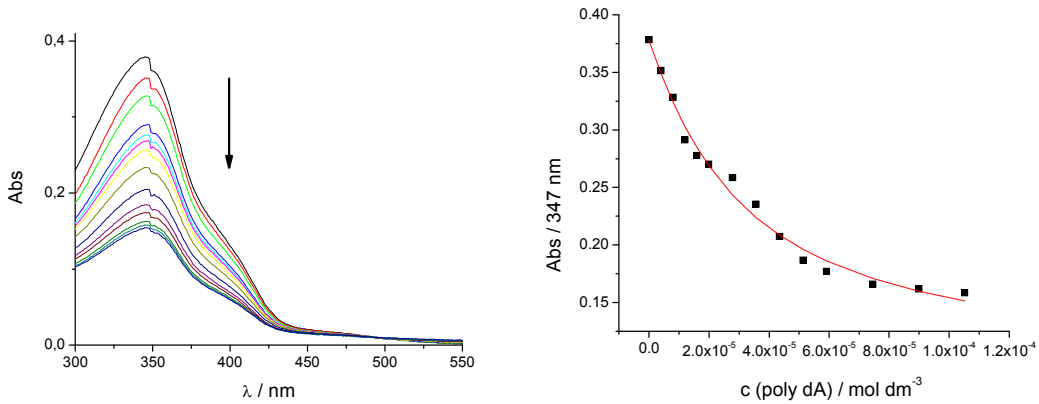

Figure S10. *Left*: Changes in UV/vis spectrum of **1** (c= 9.0 × 10^{-6} mol dm^{-3}) upon titration with poly dA (c= 4.0 × 10^{-6} – 1.0 × 10^{-4} mol dm^{-3}); *Right*: Experimental (■) and calculated data (—), processed according to the Scatchard equation, of **1** (λ_{max}=347 nm) as a function of poly dA concentration (pH=7, sodium cacodylate buffer, I = 0.05 mol dm^{-3}).

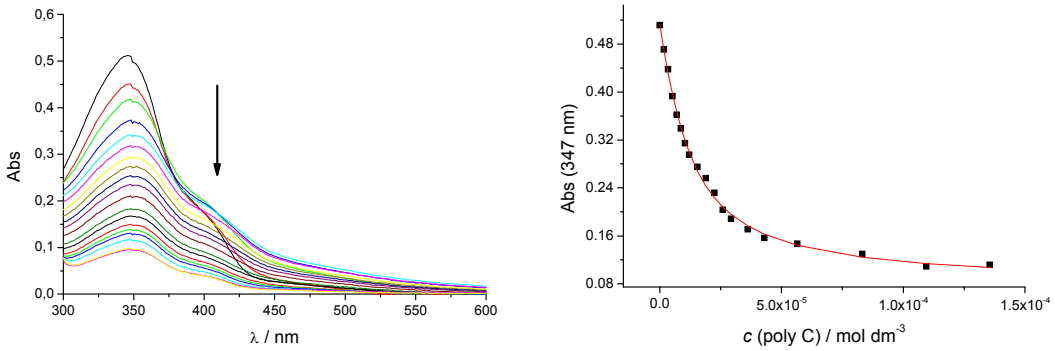

Figure S11. *Left*: Changes in UV/vis spectrum of **2** (c= 1.3 × 10^{-5} mol dm^{-3}) upon titration with poly C (c= 1.7 × 10^{-6} – 1.3 × 10^{-4} mol dm^{-3}); *Right*: Experimental (■) and calculated data (—), processed according to the Scatchard equation, of **2** (λ_{max}=347 nm) as a function of poly C concentration (pH=7, sodium cacodylate buffer, I = 0.05 mol dm^{-3}).

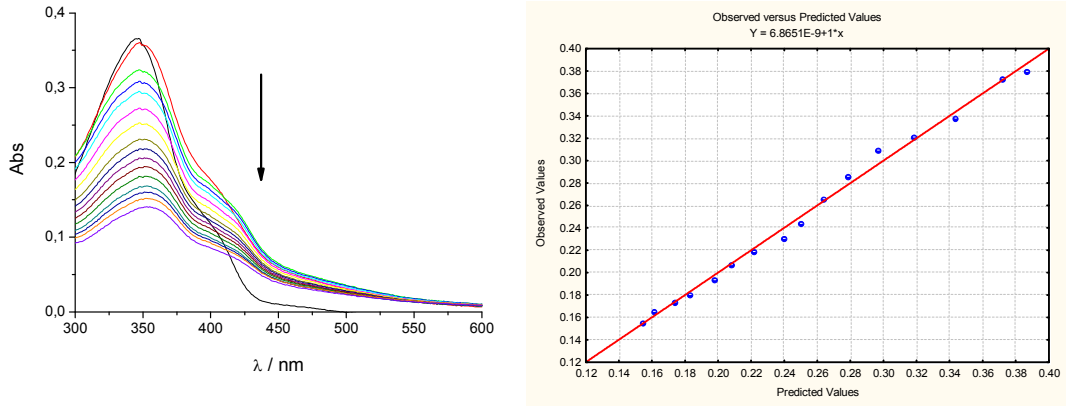

Figure S12. *Left*: Changes in UV/vis spectrum of **2** (c= 8.4 × 10^{-6} mol dm^{-3}) upon titration with poly A (c= 1.9 × 10^{-6} – 1.4 × 10^{-4} mol dm^{-3}); *Right*: Experimental (○) and calculated data (—), processed according to the Scatchard equation, of **2** (λ_{max}=346 nm) as a function of poly A concentration (pH=7, sodium cacodylate buffer, I = 0.05 mol dm^{-3}).

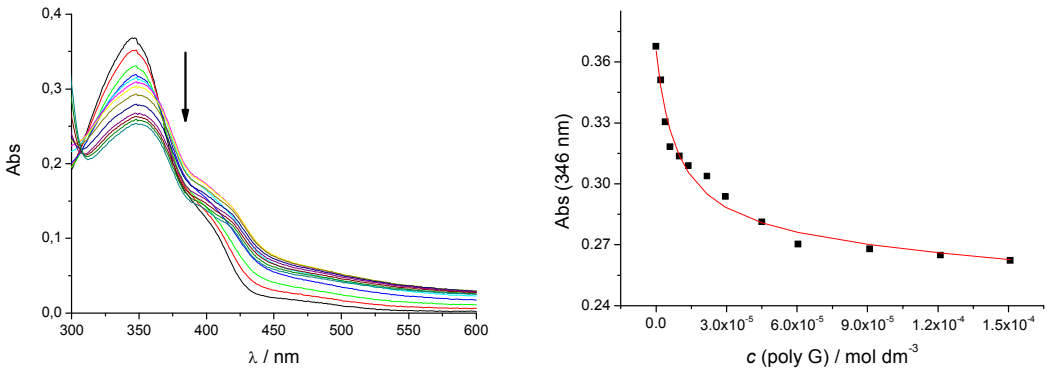

Figure S13. *Left*: Changes in UV/vis spectrum of **2** (c= 9.9 × 10^{-6} mol dm^{-3}) upon titration with poly G (c= 1.9 × 10^{-6} – 1.5 × 10^{-4} mol dm^{-3}); *Right*: Experimental (■) and calculated data (—), processed according to the Scatchard equation, of **2** (λ_{max}=346 nm) as a function of poly G concentration (pH=7, sodium cacodylate buffer, I = 0.05 mol dm^{-3}).

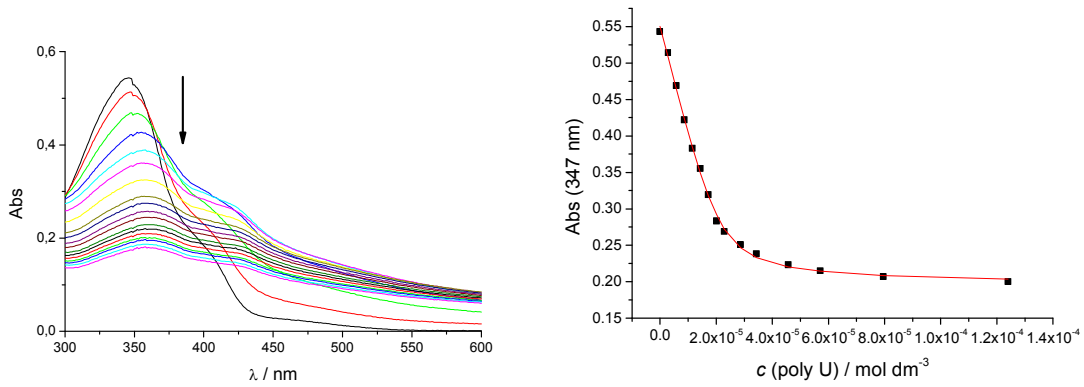

Figure S14. *Left*: Changes in UV/vis spectrum of **2** (c= 1.3 × 10^{-6} mol dm^{-3}) upon titration with poly G (c= 2.9 × 10^{-6} – 2.5 × 10^{-4} mol dm^{-3}); *Right:* Experimental (■) and calculated data (—), processed according to the Scatchard equation, of **2** (λ_{max}=347 nm) as a function of poly G concentration (pH=7, sodium cacodylate buffer, I = 0.05 mol dm^{-3}).

3.5. Competitive CD experiment with poly dT and poly U

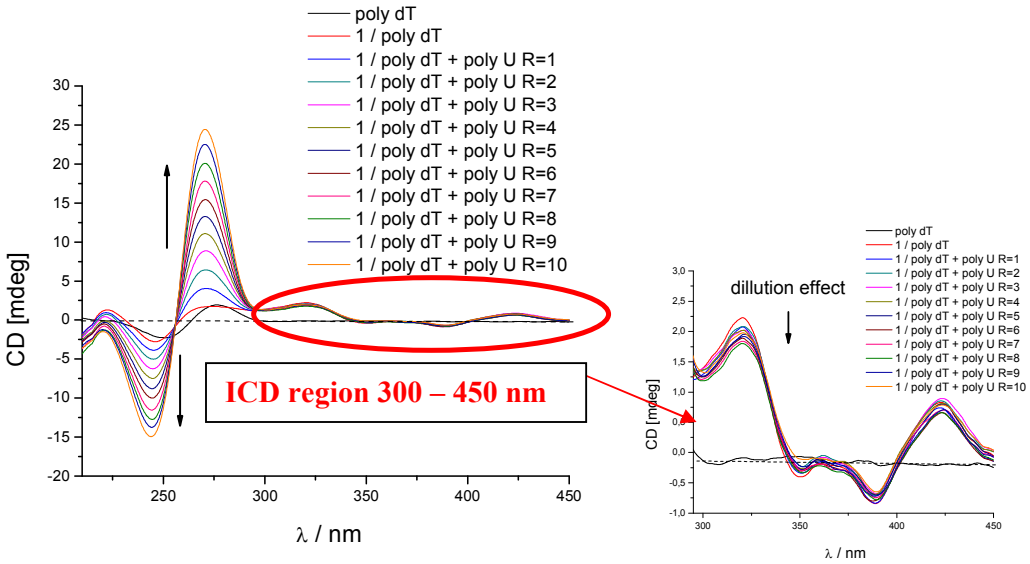

Figure S15. Changes in the CD spectra of **1**/poly dT complex (c(poly dT) = 1.5 × 10^{-5} mol dm^{-3}; c(**1**) = 7.5 × 10^{-6} mol dm^{-3}), upon addition of an 1-10-fold excess of poly U (R= [poly U]/ [poly dT]). Done at pH 7.0, buffer sodium cacodylate, I = 0.05 mol dm^{-3}. **Increase of CD bands at 245 nm and 275 nm corresponds to intrinsic CD spectrum of poly U.**

3.6. UV/vis and CD experiment of 1 with deka dT, titrations with mononucleotides

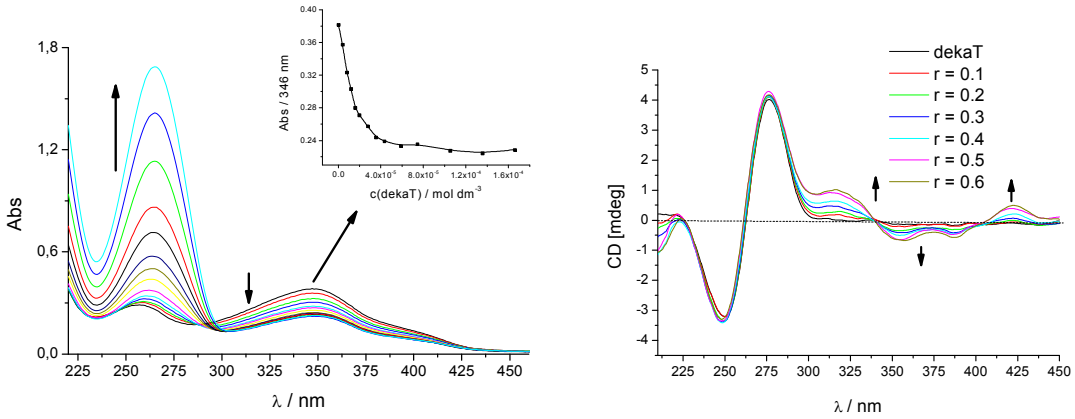

Figure S16a. *Left*: Changes in the UV/vis spectrum of **1** (c = 9.0 × 10^{-6}mol dm^{-3}) upon addition of dekadT. Inset: Dependence of **1** absorbance at λ_{max}= 346 nm on the concentration of dekadT. *Right:* Changes in the CD spectrum of deka dT (c = 3.0 × 10^{-5}mol dm^{-3}) upon addition of **1** at molar ratios ***r*** = [compound]/ [polynucleotide] (pH 7.0, buffer sodium cacodylate, I = 0.05 mol dm^{-3}).

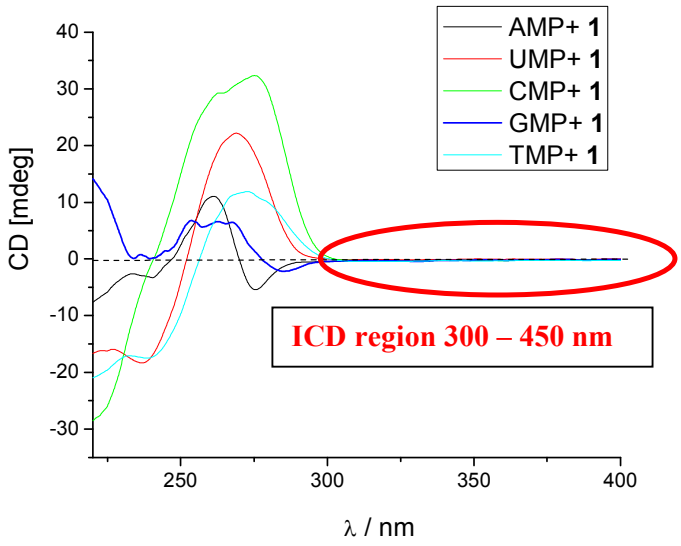

Figure S16b. CD titration of **1** (c= 1.0× 10^{-5} mol dm^{-3}) with AMP, GMP, CMP, UMP and TMP (c= 2.0 × 10^{-4} mol dm^{-3}) at pH 7.0, buffer sodium cacodylate, I = 0.05 mol dm^{-3}.

Table S2. Binding constants (log*Ks*)[a,b] for **1**/nucleotide[d] complexes calculated from the UV/Vis titrations at pH 7.0 (buffer sodium cacodylate, I = 0.05 moldm^{-3})

AMP		GMP		CMP		UMP		TMP	
log*Ks*	[c] H/%	log*Ks*	[c] H/%	log*Ks*	[c] H/%	log*Ks*	[c] H/%	log*Ks*	[c] H/%
4.7	20.9	5.0	21.7	4.9	21.7	4.8	20.2	4.9	23.7

[a]Titration data were processed according to the Scatchard equation; all log*Ks* values were calculated for fixed n=1 (stoichiometry 1 : 1);
[b]Accuracy of $n\pm$ 10 - 30%, consequently log*Ks* values vary in the same order of magnitude;
[c]H=(Abs(**1**) - Abs(complex)) / Abs(**1**)x 100;
[d]AMP = adenosine monophosphate; GMP = guanosine monophosphate; CMP = cytidine monophosphate; UMP = uridine monophosphate; TMP = thymidine monophosphate.

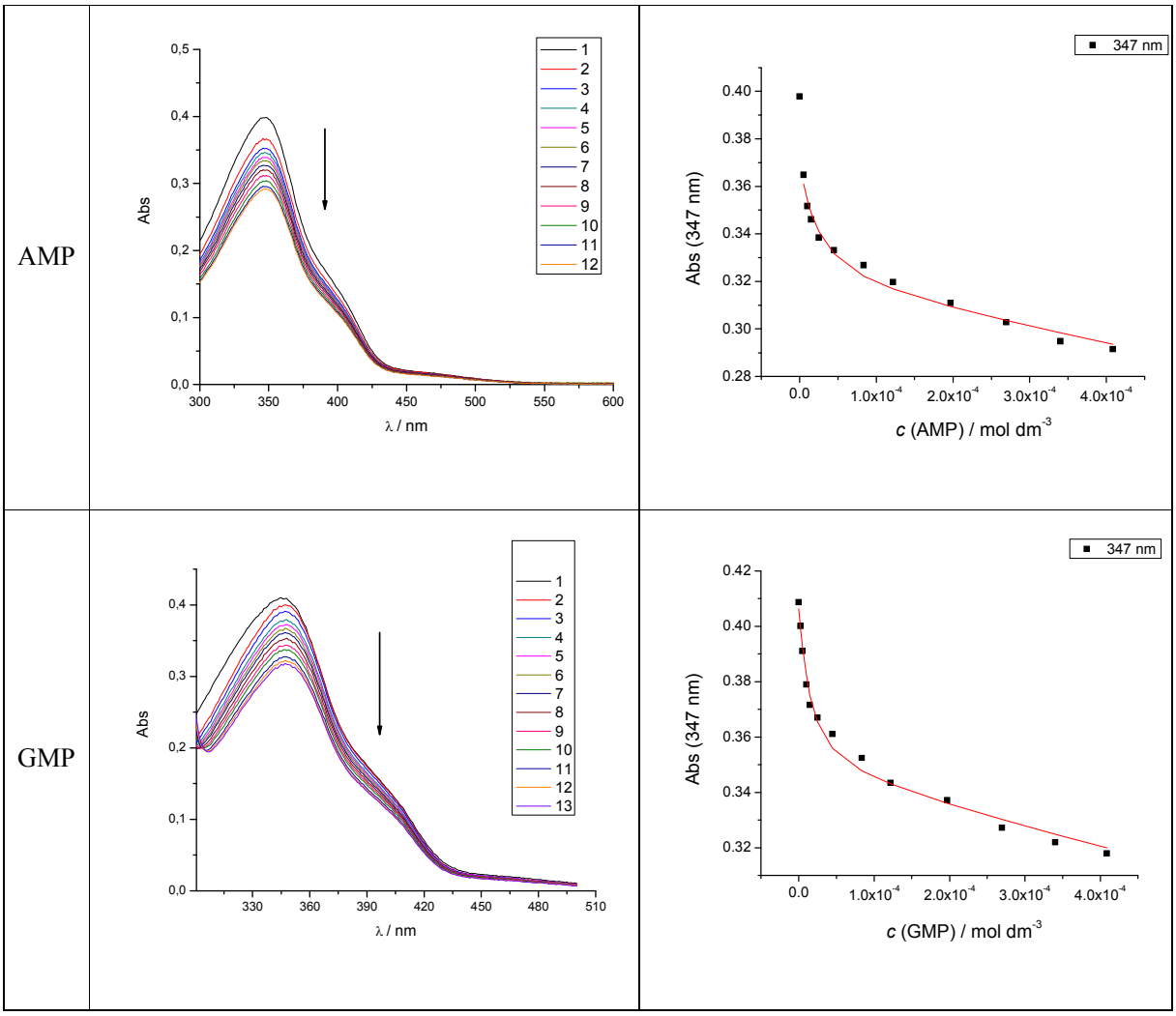

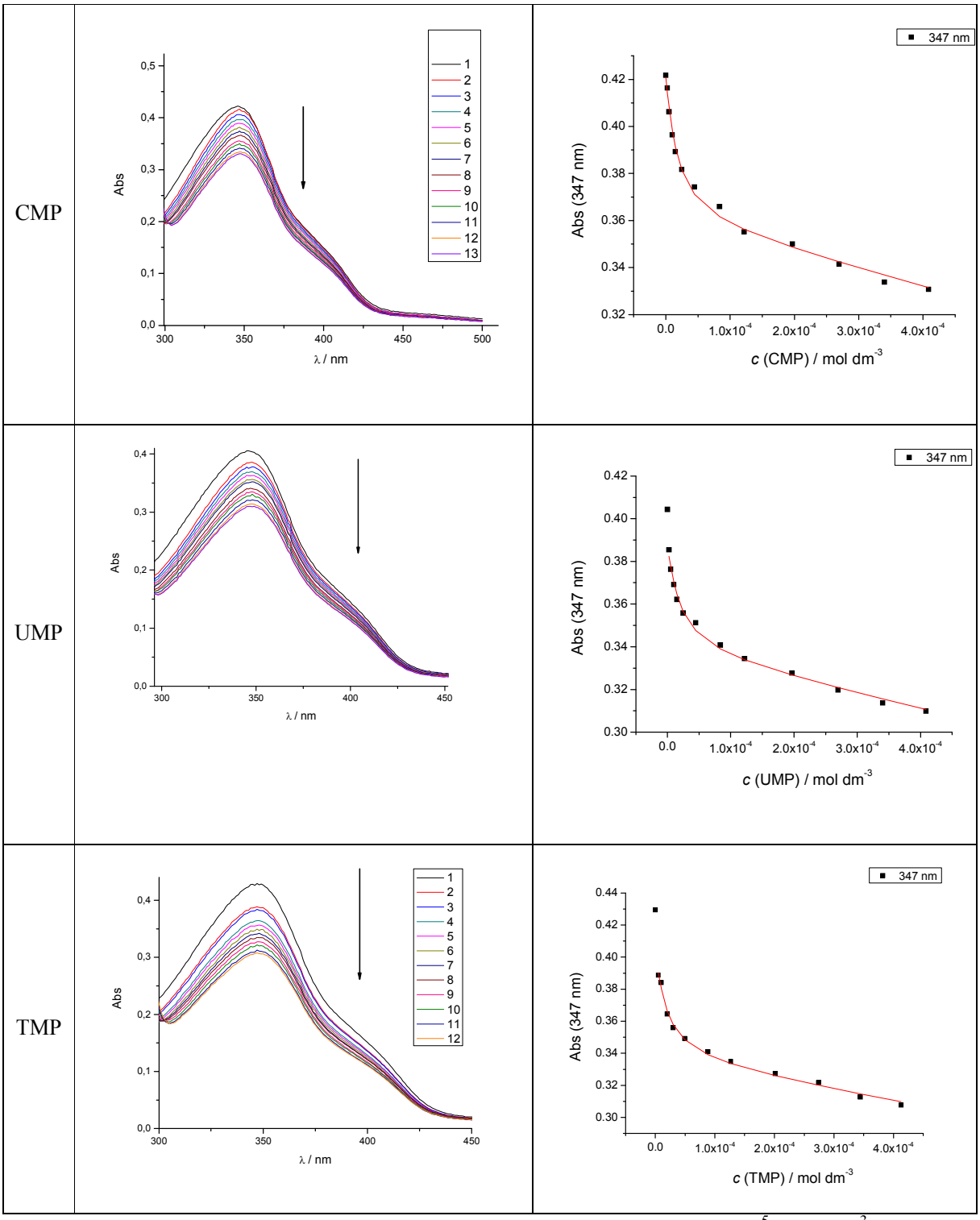

Figure S16c. *left column*) Changes in UV/vis spectrum of **1** (c= 1.0× 10^{-5} mol dm^{-3}) upon titration with AMP, GMP, CMP, UMP and TMP (c= 5× 10^{-6}– 4.0× 10^{-4} mol dm^{-3}); *right column*) Dependence of **1** absorbance at λ_{max} = 347 nm on c(AMP, GMP, CMP, UMP and TMP), at pH=7, sodium cacodylate buffer, I = 0.05 mol dm^{-3}.

4 Molecular modelling: Method and Results

Method

Single stranded tetranucleotides, DNA (poly dT) and RNA (poly rU) were built with the program *nucgen*, a part of the Amber program suit.[4] Compounds **1** and **3** were built using module 'Builder' within program *InsightII*. [5] Complexes with ss-polynucleotides were built by intercalating the aromatic ring of DBTAA into the space between two adjacent bases in the middle of the polynucleotides. The adenine of **1** was oriented in the way form two H-bonds with the polynucleotide-base, (thymine and uracil in the complex with ss-DNA and ss-RNA, respectively).

Parameterization was performed within the AMBER ff99SB force filed of Duan et al.[6] and the general AMBER force field GAFF. Each complex was placed into the center of the octahedral box filled with TIP3 type water molecules, a water buffer of 7 Å was used, and Na^+ ions were added to neutralize the systems. The solvated complexes were geometry optimized using steepest descent and conjugate gradient methods, 2500 steps of each. The optimized complexes were heated in steps of 100 K, each lasting 200 ps, while the volume was kept constant. The equilibrated systems were subjected to 3 ns of the productive unconstrained molecular dynamics (MD) simulation at constant temperature and pressure (300 K, 1 atm) using Periodic Boundary Conditions (PBC). The time step during the simulation was 1 fs and the temperature was kept constant using Langevin dynamics with a collision frequency of 1 ps^{-1}. The electrostatic interactions were calculated by the Particle Mesh Ewald (PME) method with cutoff-distance of 11 Å for the pairwise interactions in the real space. Geometry optimization and molecular dynamics (MD) simulations were accomplished using the AMBER 9 program package.

Results

In the initial complexes between **1** and ss poly-nucleotides (poly dT poly rU)) the substrate was oriented in the similar way with its rings stacked but enabling formation of the hydrogen bonds between adenine and either thymine or uracil (Figures S17 and S18). The complexes were solvated, energy optimized, and subjected to MD simulations. The complex between ss-DNA and **3** was built from the **1**-ss-DNA complex by removing adenine. The initial aromatic stacking between DBTAA and nucleobases of the complexes was not disrupted during the 3 ns of MD simulations at room temperature. However, analysis of the results of MD simulations showed that the complex of **1** with ss-DNA is more stable than the complex with ss-RNA. Besides the aromatic stacking of DBTAA with thymines, one hydrogen bond between adenine and thymine was preserved (green line in Figure 4 in the manuscript), while this was not the case in the complex with ss-RNA (see Figure S18). In Figure S18 on the right side we can see that there are no hydrogen bonds retained between adenine and uracil.

Application of the identical modelling approach to the reference compound **3** revealed a completely different binding mode (Figure S19) whereby **3** does not have adenine to form H-bonds with thymine and in addition the contact of T-methyl with 3-pyridyl is lacking.

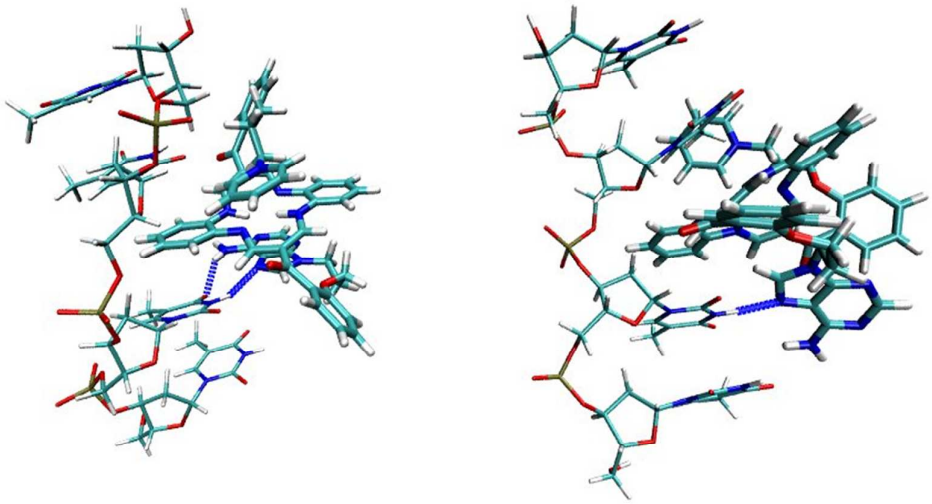

Figure S17: The **1**/poly dT complex: initial optimized (left) and final optimized structure (right).

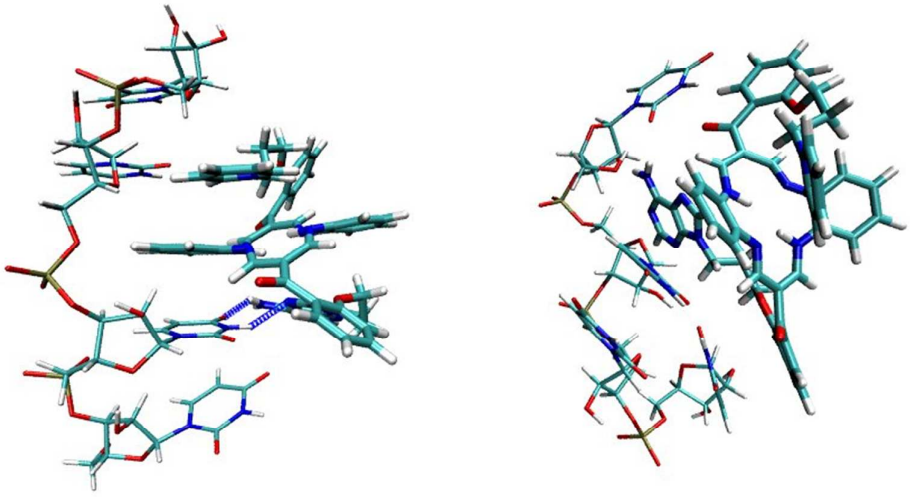

Figure S18: The **1**/poly rU complex: initial optimized (left) and final optimized structure (right).

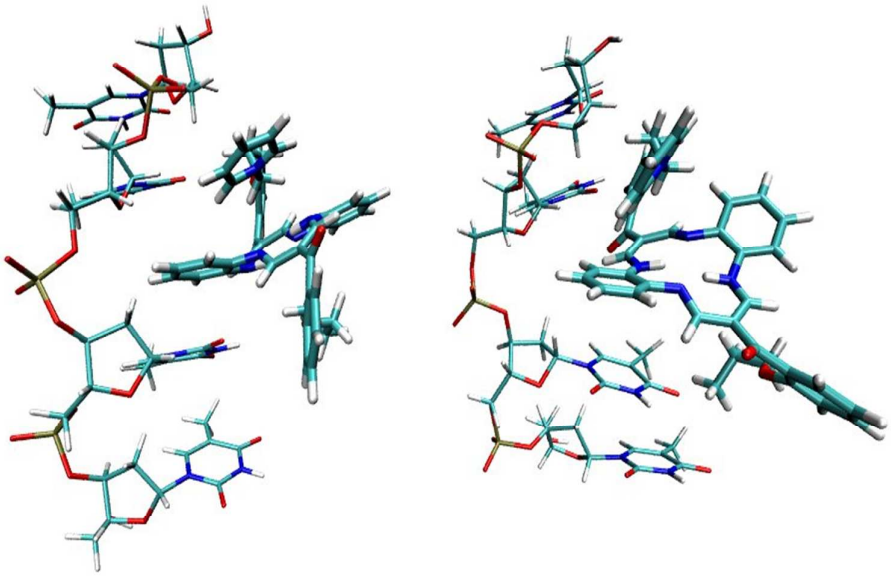

Figure S19: The **3**/poly dT complex: initial optimized (left) and final optimized structure (right).

5. References in Supp. Info.:

1 G. Cohen and H. Eisenberg, *Biopolymers*,1969, **8,** 45; M. Wirth, O. Buchardt, T. Koch, P. E. Nielsen and B. Nordén, *J. Am. Chem. Soc*., 1988, **110,** 932.

2 Y.Li, Z.Yang, *Inorg. Chim. Acta*, 2009, **362**,4823.; C.P. Tan, J. Liu, L –M. Chen, S. Shi, L–N. Ji, *J. Inorg. Biochem.*,, 2008, **102**,1644.; Q. Wang, W. Li, F. Gao, S. Li, J. Ni, Z. Zheng, *Polyhedron*, 2010, **29**, 539.; G. Zuber, J.C. Jr. Quada, S.M. Hecht, *J. Am. Chem. Soc*, 1998, **120**, 9368.

3 Z-F. Chen, L. Mao, L-M. Liu, Y-C Liu, Y. Peng, X. Hong, H-H. Wang, H-G Liu, H. Liang, *J. Inorg. Biochem.*, 2011, **105**,171.

4 http://amber.scripps.edu/

5 INSIGHTII – Accelerys San Diego 2001-2008; http://accelrys.com/services/training/life-science/insight-migration.html

6 Y. Duan, C. Wu, S. Chowdhury, M. C. Lee, G. Xiong. W. Zhang. R. Yang, P. Cipelak, R. Luo and T. Lee, *J. Comput. Chem*., 2003, **24**, 1999.